Brain, Behavior, and Immunity 133 (2026) 106248

Contents lists available at ScienceDirect

Brain Behavior and Immunity

journal homepage: www.elsevier.com/locate/ybrbi

Full-length Article

Model of selective neurodegeneration driven by a *Ccp1* mutation leads to atypical microglia with an increased response to pathological stimuli

David Pérez-Boyero [a,b], Ana de la Mata [c,d], Jesus Castillo-Sanchez [e], Ingrid Reverte [f,g], Natalia Yanguas-Casás [h], Carmelo Ávila-Zarza [i], Jorge Valero [a,b], José R. Alonso [a,b], Maria-Angeles Arevalo [h,j], Davide Ragozzino [f,g], Eduardo Weruaga [a,b,1], David Díaz [a,b,1,*]

[a] Laboratory of Neuronal Plasticity and Neurorepair, Institute of Neuroscience of Castile and Leon (INCyL), Universidad de Salamanca, 37007 Salamanca, Spain
[b] Institute of Biomedical Research of Salamanca (IBSAL), 37007 Salamanca, Spain
[c] Institute of Applied Ophthalmobiology (IOBA), Universidad de Valladolid, 47011 Valladolid, Spain
[d] Biomedical Research Networking Centre in Bioengineering, Biomaterials and Nanomedicine (CIBER-BBN), Carlos III National Institute of Health, 47011 Valladolid, Spain
[e] Cancer Cell Cycle Group, Vall d'Hebron Institute of Oncology (VHIO), 08035 Barcelona, Spain
[f] Department of Physiology and Pharmacology, Sapienza University of Rome, 00185 Rome, Italy
[g] Santa Lucia Foundation (IRCCS Fondazione Santa Lucia), 00179 Rome, Italy
[h] Spanish National Research Council (CSIC), Cajal Institute, 28002 Madrid, Spain
[i] Department of Statistics, Universidad de Salamanca, 37007 Salamanca, Spain
[j] CIBER of Frailty and Healthy Aging (CIBERFES), Carlos III National Institute of Health, 28029 Madrid, Spain

ARTICLE INFO

Keywords:
Cytoskeleton
Immune response
Microglia
Microgliosis
Motor behaviour
Neurodegeneration
Neuroinflammation

ABSTRACT

Microglia are the primary immune cells of the central nervous system and maintain tissue homeostasis through phagocytosis and regulation of inflammatory signalling. Although these functions are well established, the molecular mechanisms that control microglial activation during neurodegeneration remain poorly understood. We focused on the Purkinje Cell Degeneration (PCD) mouse, which carries a loss-of-function mutation in *Ccp1* that disrupts tubulin post-translational modifications essential for cytoskeletal stability. Because cytoskeletal dynamics are fundamental for microglial motility, phagocytosis, and proliferation, the *Ccp1* mutation offers a model to directly examine how intrinsic cytoskeletal defects alter microglial behaviour and how these alterations manifest within regions undergoing distinct patterns of neurodegeneration.

To this end, we combined *in vitro* and *in vivo* approaches. Microglia were isolated from neonatal cortex and adult cerebellum and olfactory bulb, and microglia-like cells were generated from bone marrow-derived haematopoietic stem cells. *In vivo* microglial depletion was achieved with the CSF1R inhibitor PLX5622. Immunohistochemistry quantified microglial density, morphology, and marker expression; transcriptomic profiling assessed identity and functional pathways; and functional assays evaluated phagocytosis, motility, and proliferation. Motor behaviour tests were performed to determine whether microglial dysfunction contributes to circuit-level impairments. Statistical analyses used parametric or non-parametric tests according to distribution.

Ccp1-deficient microglia exhibited intrinsic deficits in phagocytosis, motility, and proliferation, independent of overt neuronal loss. These impairments were amplified in degenerating regions, where microglia adopted a predominantly anti-inflammatory rather than pro-inflammatory activation profile. This atypical state suggests a

Abbreviations: **ANOVA**, Analysis of Variance; **BMDML**, Bone Marrow Derived Microglia-Like; **CB**, Calbindin D-28 k; **CCL2**, Chemokine (c-c motif) ligand 2; **CCP1**, Cytosolic carboxypeptidase 1; **CCR2**, Chemoattractant receptor 2; **CD200**, Cluster of differentiation 200; **CD200R**, Cluster of differentiation receptor 200; **CONDCA**, Childhood-Onset NeuroDegeneration with Cerebellar Atrophy; **CX3CL1**, Fractalkine/cx3c chemokine ligand 1; **CX3CR1**, Fractalkine/cx3c receptor 1; **DAPI**, 4′,6-Diamidino-2-phenylindole; **DPBS**, Dulbecco's Phosphate Buffered Saline; **EDTA**, Ethylene Diamine Tetraacetic Acid; **EPL**, External Plexiform Layer; **FBS**, Fetal Bovine Serum; **GAPDH**, GlycerAldehyde-3-Phosphate Dehydrogenase; **GL**, Glomerular Layer; **GrL**, Granular Layer; **iNOS**, Inducible Nitric Oxide Synthase; **IPL**, Inner Plexiform Layer; **MCL**, Mitral Cell Layer; **ML**, Molecular Layer; **OB**, Olfactory Bulb; **PB**, Phosphate Buffer; **PBS**, Phosphate Buffered Saline; **PCD**, Purkinje Cell Degeneration; **PCL**, Purkinje Cell Layer; **PCR**, Polymerase Chain Reaction; **qPCR**, quantitative PCR; **SD**, Standard Deviation; **CNS**, Central Nervous System; **TLR**, Toll Like Receptors; **TNF-α**, Tumor Necrosis Factor α; **WT**, Wild-Type.

* Corresponding author.
E-mail address: ddiaz@usal.es (D. Díaz).
[1] These authors have contributed equally to this work.

https://doi.org/10.1016/j.bbi.2025.106248
Received 13 September 2025; Received in revised form 26 December 2025; Accepted 27 December 2025
Available online 29 December 2025

maladaptive response that may compromise tissue homeostasis and intensify disease progression. Consistent with this, animals showed altered motor behaviour, indicating functional consequences of microglial dysfunction.

Together, these findings identify *Ccp1* as a key regulator of microglial homeostasis and demonstrate how cytoskeletal disruption can reshape microglial responses in neurodegenerative environments, providing mechanistic insight and potential therapeutic targets.

1. Introduction

Neurodegenerative disorders involve widespread neuronal death affecting movement, cognition, and/or affectivity, among other functions (Wes et al., 2016). Alongside this neuronal loss, activation of the immune system—particularly microglia—is triggered, leading to inflammation that, if excessive, can exacerbate primary neuronal loss (Li et al., 2014). Furthermore, some studies suggest that microglia dysfunction may even act as a trigger for the pathological processes underlying certain neurodegenerative diseases (Mhatre et al., 2015; Cheng et al., 2020; Wu & Zou, 2022; Bhusal et al., 2023). Thus, investigating the immune response within the central nervous system (CNS) and the role of microglia in neurodegeneration and neuroinflammation represents a major challenge in contemporary neuroscience (Wes et al., 2016; Salter & Stevens, 2017). A comprehensive understanding of microglia activity in disease contexts could facilitate the identification of novel therapeutic targets (Goldmann & Prinz, 2013).

Numerous animal models are employed to study the neurodegenerative and neuroinflammatory processes underlying various neurological pathologies (Pasko et al., 2023). In our study, we utilized the Purkinje Cell Degeneration (PCD) mutant mouse, a model of the human disorder known as childhood-onset neurodegeneration with cerebellar atrophy (CONDCA), which is associated with loss-of-function mutations of the *cytosolic carboxypeptidase 1* gene (*Ccp1*; Fernandez-Gonzalez et al., 2002; Wang & Morgan, 2007; Shashi et al., 2018; Karakaya et al., 2019). This pathology leads to selective postnatal degeneration of Purkinje cells in the cerebellum at around postnatal day 25 (P25), and to the death of mitral cells in the olfactory bulb (OB) by approximately P70 (Fernandez-Gonzalez et al., 2002; Valero et al., 2007; Wang & Morgan, 2007). Accompanying this neuronal loss, distinct processes of microgliosis are triggered in both the cerebellum and OB of PCD mice (Baltanás et al., 2013). Specifically, in the cerebellum, exacerbated microgliosis is observed during early postnatal weeks, whereas in the OB, a more moderate microgliosis emerges at later, more adult stages (Baltanás et al., 2013). This variability makes the PCD mouse an ideal model for studying microglial dynamics, as microgliosis and neuroinflammation occur in distinct brain regions, at different ages, and with varying degrees of severity within the same animal (Valero et al., 2006; Valero et al., 2007; Baltanás et al., 2013). Moreover, the role of the *Ccp1* gene in microglial function remains unknown, and it is still unclear whether its absence affects microglial function as it is highly expressed in this cell type (Baltanás et al., 2021; Human Protein Atlas, 2025).

Previous studies have demonstrated that microglial dysfunction and exacerbated immune responses may contribute to the progression of neurodegenerative disorders (Mhatre et al., 2015; Cheng et al., 2020; Bhusal et al., 2023). Within this framework, the present study examines microglial activity under physiological and pathological conditions. Specifically, we sought to investigate the role of microglia in the PCD mouse model, with particular emphasis on how alterations in microglial function may influence neurodegenerative processes. We first aimed to examine the impact of microglial depletion during the phase of maximal cerebellar neurodegeneration in PCD mice. Furthermore, to explore the mechanisms underlying microglial dysregulation, we conducted a comprehensive characterisation of microglial properties and functions using both *in vitro* and *in vivo* approaches. For the *in vitro* analyses, we employed bone marrow-derived microglial-like (BMDML) cells from wild-type (WT) and PCD mice, as well as microglia isolated from the cerebral cortex, cerebellum, and OB of both genotypes. In parallel, *in vivo* analyses were performed in the cerebellum and OB of WT and PCD mice at different stages of disease progression—before, during, and after the onset of neurodegeneration—to assess how distinct neurodegenerative environments shape microglial responses.

In this context, a detailed understanding of microglial function across different pathological environments is essential, as alterations in core microglial processes such as phagocytosis, motility, and immune signalling may critically influence the onset and progression of neurodegenerative disorders. The PCD mouse therefore represents a valuable experimental model to investigate the potential contribution of microglial dysfunction to region-specific and stage-dependent neurodegenerative processes within the same organism.

2. Methods

2.1. Experimental animals and genotyping

Mice (Mus musculus L., 1758; Muridae, Rodentia, Mammalia) of the C57BL/DBA strain (Bar Harbor, ME, USA) were used for all experiments. All animals were handled in compliance with current European (Directive 2010/63/EU and Recommendation 2007/526/EC) and Spanish (Royal Decree 53/2013 and Law 32/2007) regulations, with the corresponding approval of the Bioethics Committee of the University of Salamanca (reference #00613).

PCD mice are not suitable for breeding (Wang & Morgan, 2007). Therefore, the colony was maintained by mating heterozygous animals, which are indistinguishable from their WT littermates. Consequently, all offspring were genotyped by PCR as previously described (Valero et al., 2006; Díaz et al., 2012). Animals were grouped according to genotype and age at the time of analysis (n = 4-8 animals per experimental group; see Experimental design). Males and females were indistinctly used in this study since no dimorphic differences have been reported for the variables considered (Wang & Morgan, 2007).

2.2. Experimental design

The experimental design in this study adhered to the 3Rs principle of animal research—Replacement, Reduction, and Refinement—as proposed by Russell and Burch (Russell & Burch, 1959). This approach ensured the use of the minimum number of animals to obtain robust, conclusive, and reproducible results. It should be noted that, for all *in vitro* experiments, cells obtained from two animals were pooled to generate one experimental sample, which was subsequently considered a single independent experimental unit (n = 1) for data analysis, as cell numbers from individual animals were insufficient to complete all planned assays.

Microglia were eliminated from the cerebellum by treating 4 PCD mice with a microglial inhibitor at P25, corresponding to the peak of Purkinje cell degeneration. These animals were compared with 4 WT mice and 4 untreated PCD mice. The objective was to analyse the impact of microglia activity on the maximal neurodegenerative phase in the PCD mouse model. In parallel, motor behaviour tests were performed at P25 (n = 5 per group) to determine whether microglial activation exacerbates the motor impairments observed in PCD mice.

To analyse BMDML cells, 8 WT and 8 PCD mice at P25 were used. In this experiment, the objective was to analyse the effect of *Ccp1* gene expression on the physiological state of microglia in the absence of direct neuronal influence. The use of BMDML cells allows the assessment

of intrinsic alterations associated with the *Ccp1* mutation independently of neuronal signals or region-specific neural microenvironments, enabling the identification of microglia-intrinsic functional changes.

For the analysis of cortical microglia from neonatal mice, 8 WT and 8 PCD mice aged between P2-P4 were used. Likewise, the effect of *Ccp1* gene expression on the physiological state of microglia in the absence of direct influence of degeneration was assessed. Microglia isolated at this early postnatal stage were analysed after *in vivo* exposure to a neural environment, but prior to the onset of overt neurodegeneration in the PCD model, allowing the study of *Ccp1*-associated microglial alterations under relatively healthy neural conditions and during early developmental stages.

To analyse adult microglia, isolated from the cerebellum and OB, 8 WT mice and 8 PCD mice were used at P25 and P70, respectively (16 animals of each genotype in total). The effect of *Ccp1* gene expression on the pathological state of microglia within the neurodegenerative environment characteristic of the PCD mouse was assessed. These regions were selected due to their differential vulnerability in the PCD model, allowing the evaluation of microglial responses following prolonged interaction with region-specific neurodegenerative environments during disease progression.

A total of 24 WT and 24 PCD mice at P15, P25, and P40 (corresponding to stages before, during, and after Purkinje cell neurodegeneration, respectively) were used to study cerebellar microglia *in vivo*. For the *in vivo* analysis of OB microglia, 24 WT and 24 PCD mice were used at the ages of P40, P70, and P120 (corresponding to stages before, during, and after mitral cell neurodegeneration, respectively). In this case, the objective was to analyse the direct effect of the neurodegenerative environment in PCD mice on microglia biology, while also comparing two distinct severities of neuronal cell death.

2.3. Microglial inhibitor administration and analysis of motor behaviour

The microglial inhibitor PLX5622 (MedChemExpress, Monmouth Junction, NJ, USA; Spangenberg et al., 2019; Riquier & Sollars, 2020; Basilico et al., 2022) was administered systemically via intraperitoneal injection. Due to its low solubility, PLX5622 was dissolved in corn oil (MedChemExpress), which was used as the vehicle for all treatments. Administration via chow was not feasible in this study, as treatment needed to begin before weaning and animals at this age do not consume solid food independently; therefore, intraperitoneal delivery was required.

Treatment was initiated prior to the onset of Purkinje cell degeneration, starting at P15, and continued until P24, coinciding with the period of maximal vulnerability and peak degeneration in the PCD model. The choice of P15 as the starting point was based on both welfare and biological considerations, as critical events of cerebellar organisation and circuit formation occur between P10 and P15 (Sillitoe & Joyner, 2007; Hashimoto & Kano, 2013), and pharmacological intervention during this window was avoided. A total of four doses were administered at a concentration of 50 mg/kg, with injections performed every 72 h.

The dosing regimen was established based on pilot optimisation experiments aimed at achieving an effective reduction of microglial cells while preserving animal welfare. Regimens involving earlier starting ages or higher injection frequencies resulted in significant adverse effects, including weight loss, lethargy, and increased mortality, and were therefore excluded. In contrast, administration every 72 h from P15 was well tolerated, with no signs of distress, behavioural alterations, or reductions in body weight. Under these conditions, PLX5622 treatment induced a marked reduction in microglial density, without resulting in complete microglial ablation, consistent with previous reports indicating that short-term CSF1R inhibition leads to partial depletion and that extended treatment is required for near-complete elimination (Spangenberg et al., 2019; Kodali et al., 2025).

At P25, animals were sacrificed and cerebellar tissue was collected for immunohistochemical analysis. The expression of Iba1 was used to assess microglial abundance, while Calbindin D-28 k was used as a marker of Purkinje cells (see Table 1). In addition, motor coordination and balance were assessed prior to sacrifice at P25 using the rotarod test. Motor performance was quantified by measuring the latency to fall, defined as the time each mouse was able to remain on the accelerating rotating rod before falling. All behavioural assessments were conducted under identical experimental conditions across groups.

2.4. Bone marrow-derived microglial-like cell cultures

Bone Marrow Haematopoietic Stem Cells (BMHSCs) were differentiated into BMDML cells as previously described (Servet-Delprat et al., 2002; Hinze & Stolzing, 2011; Hinze & Stolzing, 2012) with minor modifications (see Supplementary Methods). Briefly, mice were euthanised by cervical dislocation, and their femurs, tibias, and ilia were harvested. BMHSCs were extracted by injecting Dulbecco's Modified Eagle Medium (DMEM, Sigma-Aldrich, St. Louis, MO, USA) into the epiphyses. Cells were then cultured in low-glucose complete DMEM supplemented with 10 % (v/v) foetal bovine serum (FBS; Hyclone cytiva, Logan, UT, USA) and 1 % (v/v) penicillin/streptomycin (P/S; Lonza, Pontevedra, Spain). Cells were seeded in 75 cm^2 flasks (Thermo Fisher Scientific, Waltham, MA, USA) pre-coated with poly-L-lysine (50 μg/mL; Sigma-Aldrich), and maintained for 10 days, the period required for the proper differentiation of BMHSCs into BMDML cells.

The microglial identity and purity of BMDML cultures were routinely assessed prior to experimental use by Iba1 immunocytochemistry, and only cultures showing a high proportion of Iba1-positive cells without detectable contamination from other cell lineages were included in the study.

2.5. Cortical microglia cultures

Cortical microglia were obtained as previously described (Bronstein et al., 2013; Daniele et al., 2014). Neonatal mice were euthanised by decapitation, and their cerebral cortices were dissected, homogenised, and cultured in DMEM/F-12 medium (Sigma-Aldrich) supplemented with 10 % (v/v) FBS and 1 % (v/v) P/S. Cells were seeded into 75 cm^2 flasks, pre-coated with poly-L-lysine (10 μg/mL). Once cultures reached confluence, flasks were shaken at 200 rpm for 2 h at 37 °C to detach microglial cells. The supernatants were collected and centrifuged at 1,200 rpm for 5 min, and the resulting microglial pellets were used for subsequent experiments (gene expression analyses, immunocytochemical characterization, phagocytosis assays, motility assays, and cell proliferation/viability assays).

The purity of cortical microglial cultures was verified prior to experimental use by Iba1 immunocytochemistry, and only cultures showing a high proportion of Iba1-positive cells without detectable contamination from other neural cell types were included in the study.

2.6. Adult microglia cultures from the cerebellum and olfactory bulb

Microglia from the cerebellum and OB were isolated as previously described (Lee & Tansey, 2013). Mice were anaesthetised and transcardially perfused with 0.9 % (w/v) saline solution. The cerebella and OBs were dissected and enzymatically digested at 37 °C for 30 min with shaking at 100 rpm in a buffer containing papain, dispase II, and DNase I (Sigma-Aldrich), followed by mechanical dissociation. The reactions were neutralised, and the cells were centrifuged and filtered through a 40 μm filter (Thermo Fisher Scientific) and centrifuged at 1,200 rpm at 18 °C for 10 min; this entire step was performed twice. The pellets were resuspended in 2 mL DMEM/F-12 and 10 μL/10^7 CD11b microsphere cells (Miltenyi Biotec, Bergisch Gladbach, Germany) were added to the mixture. Magnetically labelled microglia cells were then collected using the MACS column system (Miltenyi Biotec). The purified microglia were subsequently used for various experiments.

Due to the low abundance of microglia in these brain regions, tissue

Table 1
Primary and secondary antibodies used in the indirect immunofluorescence technique for *in vitro* and *in vivo* experiments.

1° Antibody	Species	Origin	Dilution	2° Antibody	Origin	Dilution
Calbindin D-28 k (tissue)	Mouse	Swant	1:1000	Cy3 mouse anti-IgG	Jackson	1:500
CD16/32 (tissue)	Rat	BD	1:200	Cy3 rat anti-IgG	Jackson	1:500
CD206 (tissue)	Goat	R&D Systems	1:200	Cy2 goat anti-IgG	Jackson	1:500
CD45 (tissue)	Rat	Bio-Rad Laboratories	1:1000	Cy2 rat anti-IgG	Jackson	1:500
Iba1 (cell culture/tissue)	Rabbit	Wako Pure Chemical Industries	1:500/1:1000	Cy2 or Cy3 rabbit anti-IgG	Jackson	1:1000/1:500
Ki67 (cell culture)	Mouse	Abcam	1:500	Cy2 or Cy3 mouse anti-IgG	Jackson	1:1000

from two animals was pooled for each isolation. Under these conditions, each isolation yielded approximately 500,000 microglia per sample, which represented the minimum number of cells required to perform the functional assays included in this study. The purity of adult microglial cultures was verified prior to experimental use by Iba1 immunocytochemistry, and only highly enriched microglial preparations were included in the study.

2.7. Flow cytometry analyses

Flow cytometry was used to confirm the differentiation of BMDML cells from WT and PCD BMHSCs. After the differentiation period, cells were collected, centrifuged, and resuspended in phosphate-buffered saline (PBS) supplemented with 25 mM HEPES, 10 % (v/v) FBS, and 2 % (v/v) P/S. For each sample, 1×10^6 cells were used.

Cells were subsequently incubated for 30 min at 4 °C in the dark with fluorophore-conjugated antibodies directed against the microglial markers TMEM119 (FITC-conjugated; Abcam, Cambridge, UK) and Iba1 (PerCP-Cy5.5-conjugated; Abcam), at the concentrations recommended by the manufacturers. Following staining, cells were washed twice with staining buffer and recovered by centrifugation at 1,500 rpm for 5 min at room temperature. Final cell pellets were resuspended in PBS for acquisition.

Data acquisition was performed at the Cytometry Service of the University of Salamanca using a FACSCanto™ II flow cytometer (BD Biosciences, San Jose, CA, USA). The gating strategy included the exclusion of debris and cell doublets based on forward scatter (FSC) and side scatter (SSC) parameters. Data were analysed using FlowJo software (version 10.8.1). Mean fluorescence intensity (MFI) values were calculated for each marker.

2.8. Immunocytochemical and immunohistochemical analyses

Immunocytochemical analyses of microglia from different sources were conducted to determine cell morphology and size. Both parameters were quantified based on the projected cell area and the expression levels of Iba1, a general microglial marker. For this purpose, microglial cells were seeded onto 18-mm diameter glass coverslips placed in 12-well plates (VWR International, Radnor, PA, USA). Coverslips were pre-coated with poly-L-lysine (50 μg/mL), and cells were plated at a density of 50,000 cells/cm^2.

Immunohistochemical analyses were conducted on cerebellar and OB sections to assess microglial density, distribution, morphology, projected area, and Iba1 expression levels before, during, and after Purkinje and mitral cell degeneration, respectively. In these tissue-based analyses, microglia were identified based on the combined use of Iba1 immunoreactivity and their characteristic morphology and anatomical localisation within the brain parenchyma, allowing reliable discrimination from other Iba1-expressing myeloid populations. Additionally, several microglial markers, previously used to study inflammatory responses, were evaluated during peak neurodegeneration in both regions: CD45 (reactive microglial marker), CD16/32 (pro-inflammatory microglial marker), and CD206 (anti-inflammatory microglial marker; see Table 1). For this purpose, mice were anaesthetised and perfused as previously described (Pérez-Boyero et al., 2023). The cerebella and OBs were dissected and sectioned at 30 μm thickness using a sliding freezing microtome (Jung SM 2000, Leica Instruments, Nussloch, Germany), with parasagittal sections prepared for the cerebellum and coronal sections for the OB.

Once all samples were prepared, both cells and tissue sections were incubated for 24 h at 4 °C under continuous rotational shaking in medium containing 0.2 % (v/v) Triton X-100, 5 % (v/v) normal donkey serum, and the appropriate primary antibodies (see Table 1) diluted in PBS. Following incubation, samples were rinsed in PBS and incubated for 1 h at room temperature with the corresponding secondary antibodies (Table 1) under continuous rotary shaking. Ten minutes before the end of the incubation, 4′,6-diamidino-2-phenylindole (DAPI; Sigma-Aldrich) was added at a dilution of 1:10,000. Finally, samples were mounted on gelatine-coated slides and covered with anti-fading medium. Appropriate negative controls, in which primary antibodies were omitted, showed no detectable staining.

2.9. Gene analysis by quantitative PCR

Gene expression analyses were conducted to analyse the transcriptional levels of microglial markers, including general markers (*Iba1*, *Cx3cr1*, *Tmem119*) and genes associated with key microglial functions. These included markers of phagocytic activity (*Trem2*, *Dap12*, *P2ry6*, *Cd68*), motility (*Ccl2*, *Ccr2*), and innate (*Tlr2*, *Tlr4*, *CD200r*), pro-inflammatory (*Inos*, *Tnf-α*, *Il-1β*) and anti-inflammatory (*Arg1*, *Cd206*) immune responses (Sumpter et al., 2011; Baltanás et al., 2013; Doorn et al., 2015; Rossi et al., 2018; Kaiser & Feng, 2019; Yanguas-Casás et al., 2020; Pérez-Boyero et al., 2023; see Table 2).

Cultured microglial cells used for gene analysis were plated at a density of 100,000 cells/cm^2. For tissue-based gene analysis, mice were anaesthetised and transcardially perfused with 0.9 % (w/v) saline solution. The cerebellum and OB were dissected using RNase-free instruments and processed fresh. Both cultured cells and tissue samples were homogenised using an Ultra-Turrax homogeniser (IKA, Staufen, Germany), and total cytoplasmic RNA was extracted and purified using the PureLink™ RNA Mini Kit (Thermo Fisher Scientific), and the PureLink™ DNase Set (Thermo Fisher Scientific). Total RNA from each sample was reverse transcribed into complementary DNA (cDNA) using the High-Capacity cDNA Reverse Transcription Kit (Applied Biosystems, Foster City, CA, USA). Real-time quantitative PCR (RT-qPCR) assays were then performed as previously described (Pérez-Boyero et al., 2023; Pérez-Martín et al., 2023; Del Pilar et al., 2024; Hernández-Pérez et al., 2025). The *Gapdh* gene was used as an endogenous control for data normalisation (see Table 2).

2.10. Analysis of phagocytosis

Microglial cells were seeded onto 18-mm diameter glass coverslips pre-coated with poly-L-lysine (50 μg/mL) in 12-well plates at a density of 50,000 cells/cm^2. Either Cy2-labeled microspheres (0.5 μL/well; Fluoresbrite YG Carboxylate Microspheres 1.00 μm, Polysciences, Warrington, UK) or Cy3-labeled neuronal debris (0.5 μL/well) were added to the cultures. The plates were then incubated for 1 h at 37 °C in a humidified atmosphere containing 5 % (v/v) CO_2. Following incubation, the cells were washed with pre-warmed PBS (37 °C) and fixed with 4 %

Table 2
Sequences of primers used for qPCR in both *in vitro* and *in vivo* expression analyses. Abbreviations: *Arg1*, *arginase 1*; *Ccl2*, *chemokine (c-c motif) ligand 2*; *Ccr2*, *chemoattractant receptor 2*; *Cd200r*, *cluster of differentiation receptor 200*; *Cd206*, *cluster of differentiation 206*; *Cd68*, *cluster of differentiation 68*; *Cx3cr1*, *fractalkine/cx3c receptor 1*; *Dap12*, *dnax activator protein 12 kDa*; *Gapdh*, *glyceraldehyde-3-phosphate dehydrogenase*; *Iba1*, *ionized calcium binding adaptor molecule 1*; *Il-1β*, *interleukin 1 beta*; *Inos*, *inducible nitric oxide synthase*; *P2ry6*, *pyrimidinergic receptor p2y6*; *Tlr2*, *toll-like receptor 2*; *Tlr4*, *toll-like receptor 4*; *Tmem119*, *transmembrane protein 119*; *Tnf-α*, *tumour necrosis factor α*; *Trem2*, *triggering receptor expressed on myeloid cells 2*.

Gene	Sense Oligo 5‘- 3′	Antisense Oligo 5‘- 3′	References
Arg1	GCAGCAGCCGCTGGAACCCAG	GTCCCCGTGGTCTCTCACGTC	(Yanguas-Casás et al., 2020)
Ccl2	TGTTGGCTCAGCCAGATGCAGTTA	TACAGCTTCTTTGGGACACCTGCT	(Yanguas-Casás et al., 2020)
Ccr2	CTCTGCAAACAGTGCCCAGTT	AACCGAGACCTCTTGCTCCCC	(Yanguas-Casás et al., 2020)
Cd200r	CATAGGATGCATTTGTCTTTTGAAA	GCTGCATTTCATCCTCCTCAATA	(Yanguas-Casás et al., 2020)
Cd206	GGTTGGATTGAGGCCTGAAA	AACGTCCCTTTGTTTTGAACATC	(Yanguas-Casás et al., 2020)
Cd68	CTCATCATTGGCCTGGTCCT	GTTGATTGTCGTCTGCGGG	(Doorn et al., 2015)
Cx3cr1	TGTCCTTTCTCTTTGTGAACATGA	GGCGGCGGCCATCTT	(Yanguas-Casás et al., 2020)
Dap12	CGTACAGGCCCAGAGTGAC	CACCAAGTCACCCAGAACAA	(Sumpter et al., 2011)
Gapdh	GCCTATGTGGCCTCCAAGGA	GTGTTGGGTGCCCCTAGTTG	(Baltanás et al., 2013)
Iba1	GCAGGAAGAGAGGCTGGAGGGGATC	CTCTTCAGCTCTAGGTGGGTCTTCGG	(Rossi et al., 2018)
Il-1β	GGTGTGTGACGTTCCCATTA	CCGACAGCACGAGGCTTT	(Yanguas-Casás et al., 2020)
Inos	CTTTGCCACGGACGAGAC	AACTTCCAGTCATTGTACTCTGAGG	(Pérez-Boyero et al., 2023)
P2ry6	CCAGTGCCAGGTTCAGGGTGTA	GCGTCTACCGTGAGGATTTCA	(Yanguas-Casás et al., 2020)
Tlr2	TGTCCGCAATCATAGTTTCTGATG	AGCAGAGAAGTGAAGCCCCT	(Yanguas-Casás et al., 2020)
Tlr4	GGCTCCTGGCTAGGACTCTGA	TCTGATCCATGCATTGGTAGGT	(Yanguas-Casás et al., 2020)
Tmem119	CCTTCACCCAGAGCTGGTTC	GGCTACATCCTCCAGGAAGG	(Kaiser & Feng, 2019)
Tnf-α	GAAAAGCAAGCAGCCAACCA	CGGATCATGCTTTCTGTGCTC	(Yanguas-Casás et al., 2020)
Trem2	GCACCTCCAGGAATCAAGAG	GGGTCCAGTGAGGATCTGAA	(Yanguas-Casás et al., 2020)

paraformaldehyde (Sigma-Aldrich) for subsequent immunofluorescence analysis.

2.11. Analysis of cell motility

Microglial cells were seeded at a density of 25,000 cells/cm^2 in 12-well plates pre-coated with poly-L-lysine (10 μg/mL). After cell attachment, phase-contrast time-lapse images were acquired using live-cell microscopy. Three non-overlapping fields per well were recorded every 2 min over a total period of 2 h under controlled temperature and CO_2 conditions.

Microglial motility was quantified using an automated image-analysis pipeline developed in FIJI software (NIH, WI, USA). Rather than analysing directional displacement or net migration, motility was assessed based on dynamic changes in cell position and morphology over time. Specifically, two complementary parameters were extracted: (1) the total area explored by each cell during the acquisition period, reflecting the spatial extent of cell movement, and (2) cell wandering, defined as the cumulative movement inferred from changes in the projected cell area between consecutive frames. The custom FIJI macro automatically segmented individual cells in each frame, tracked them across time, and calculated motility parameters in a consistent and unbiased manner. This approach allowed the quantification of microglial motility based on continuous cellular dynamics while minimising user-dependent variability and ensuring reproducibility across experiments.

2.12. Analysis of cell proliferation

Two complementary techniques were used to study microglial proliferation. The first involved immunocytochemical detection of the proliferation marker Ki67 (see Table 1). The second employed the alamarBlue assay (Bio-Rad, Berkeley, CA, USA), a redox-sensitive dye that fluoresces and changes colour in response to metabolic activity associated with cell growth (Czekanska, 2011; Kumar et al., 2018). For the alamarBlue assay, microglial cells were seeded at a density of 20,000 cells/cm^2 in 24-well plates (VWR international), and proliferation/cell viability was monitored over 10 days. Fluorescence was measured using a microplate reader (AMR-100, Bio-Rad) at a wavelength of 470 nm, following the manufacturer’s instructions.

2.13. Microscopic visualisation and cell analysis

Microscopy was performed using different imaging systems depending on the type of analysis. For immunocytochemical, immunohistochemical, and phagocytic assays, a STELLARIS 8 confocal microscope (Leica Microsystems, Wetzlar, Germany) was used. For cell motility studies, an Axio Observer live-cell microscope (ZEISS, Oberkochen, Germany) and an AF 6500–7000 time-lapse microscope (Leica Microsystems) were used. For proliferation studies, a DMI3000 B epi-fluorescence microscope (Leica Microsystems) equipped with a DFC300 FX digital camera (1.4 MP; Leica Microsystems) was used. The FIJI software was used for all cell analyses.

2.14. Statistical analysis

All data are presented as mean ± standard deviation (SD). Four experimental subjects were used for each type of analysis in both *in vitro* and *in vivo* experiments. For the *in vitro* experiments, 10 cells were randomly selected from each subject for analysis. All analyses were performed under blinded conditions to prevent bias and ensure the objectivity and reliability of the results.

The normality and homoscedasticity of the datasets were tested using the Shapiro-Wilk and Levene’s tests, respectively. For data that met the assumptions of normality and homogeneity of variance ($p > 0.05$ for both tests), parametric tests were applied: either the Student's *t*-test or analysis of variance (ANOVA), as appropriate. Conversely, for data that violated these assumptions ($p < 0.05$ for the Shapiro-Wilk and/or Levene’s tests), non-parametric tests were used: Mann-Whitney U or the Kruskal-Wallis test. Statistical significance was set at $p < 0.05$. Results were considered significant at $p < 0.05$ (*) and highly significant at $p < 0.01$ (**).

All statistical analyses and graphical representations were performed using SPSS version 26 for Windows (IBM, Armonk, NY, USA), GraphPad Prism version 10.0.2 for Windows (GraphPad, San Diego, CA, USA), and Microsoft Excel version 2021 for Windows (Microsoft, Redmond, WA, USA).

3. Results

3.1. An exacerbated microglial reaction increases neuronal loss along with a loss of motor skills

To determine whether microgliosis is a causal factor or simply a consequence of neurodegenerative processes occurring in the PCD mouse, we eliminated microglia from the cerebellum prior to the onset of Purkinje cell degeneration. We focused on this brain region as this is where the most aggressive and pronounced neurodegenerative changes and microgliosis occur.

A higher microglial density was observed in the cerebellum of PCD mice compared to the WT and PCD mice treated with the microglial inhibitor PLX5622, two groups that presented similar values. Significant differences in microglial density were observed in cerebellar lobes I-II (WT *vs* PCD, $p = 0.021$; PCD *vs* treated PCD, $p = 0.021$), lobe V (WT *vs* PCD, $p = 0.021$; PCD *vs* treated PCD, $p = 0.021$), and lobe VIII (WT *vs* PCD, $p = 0.021$; PCD *vs* treated PCD, $p = 0.043$). In contrast, lobe X showed no significant differences among the three experimental groups (Fig. 1), which may be attributed to its distinct degenerative pattern (see Discussion). These results indicate that PLX5622 administration significantly reduces microglia density in the cerebellum of PCD mice, restoring levels comparable to those observed in the cerebellum of WT mice.

Regarding the analysis of Purkinje cells, WT mice showed a higher neuronal density compared to both PCD and treated PCD mice, and treated PCD mice presented a higher Purkinje cell density than untreated PCD animals. Specifically, these differences in Purkinje cell density were observed in lobes I-II (WT *vs* PCD, $p = 0.021$; WT *vs* treated PCD, $p = 0.021$), lobe V (WT *vs* PCD, $p = 0.021$; WT *vs* treated PCD, $p = 0.021$; PCD *vs* treated PCD, $p = 0.021$) and lobe VIII (WT *vs* PCD, $p = 0.021$; WT *vs* treated PCD, $p = 0.021$; PCD *vs* treated PCD, $p = 0.021$). Conversely, in lobe X, similar values were observed for all three experimental groups (Fig. 1). Thus, the elimination of microglia improves the survival of these neurons in the cerebellum of PCD mice, resulting in neuronal density values that are intermediate between those found in the cerebellum of WT and untreated PCD mice.

These findings show that microglia play a critical role in the progression of the associated pathology in the PCD mouse model and that their dysfunction and/or exacerbation increases Purkinje cell death.

After conducting behavioural tests, it was observed that WT mice performed better in motor behaviour tests compared to PCD and PCD mice treated with PLX5622. Specifically, it was confirmed that WT mice had a longer fall latency than the other two groups (WT *vs* PCD, $p = 0.007$; WT *vs* treated PCD, $p = 0.007$). In addition, it was observed that PCD animals treated with PLX5622 performed better than untreated PCD animals (PCD *vs* treated PCD, $p = 0.007$). Therefore, the elimination of microglia from PCD mice improves their motor behaviour, making it more like that of WT mice.

These findings demonstrate that microglia play a key role in the progression of pathology associated with PCD in the mouse model and that their dysfunction and/or exacerbation increases Purkinje cell death and, consequently, the loss of motor skills.

3.2. Microglia derived from bone marrow haematopoietic cells of PCD mice exhibit altered gene and protein expression, decreased phagocytic capacity, and increased cell motility and proliferation

Prior to functional analyses, the differentiation of BMDML cells was verified by flow cytometry. Both WT and PCD BMDML cultures showed expression of established microglial markers, confirming successful differentiation before subsequent experiments were performed (see Supplementary Fig. S1).

Our next objective was to determine whether the *pcd* mutation directly affects microglial function. To achieve this, we designed an experiment to identify cells unaffected by any neurodegenerative process. Specifically, we studied BMDML cells, which originate from non-neural tissue (see Methods section) and are therefore free from both degenerative changes and direct neural influence.

Gene expression analysis revealed that WT BMDML cells exhibited higher expression of genes associated with general microglial markers (*Iba1*, *Cx3cr1*, *Tmem119*), phagocytosis (*Trem2*, *P2ry6*), and an anti-inflammatory immune response (*Cd206*; Fig. 2A); therefore, these cells exhibited a more anti-inflammatory microglial phenotype. Conversely, BMDML cells from PCD mice showed elevated expression of genes related to motility (*Ccl2*) and a pro-inflammatory immune response (*Tnf-α*, *Il1-β*) (Fig. 2A) and, in this case, exhibited a more pro-inflammatory microglial phenotype.

Immunohistochemical analysis revealed no significant morphological differences between WT and PCD BMDML cells (ameboid, $p = 1$; one branch, $p = 0.661$; two branches, $p = 0.767$; three or more branches, $p = 0.297$; Fig. 2D). Similarly, the average cell area did not differ significantly between WT and PCD BMDML cells ($p = 0.353$; Fig. 2E). However, WT cells exhibited significantly higher expression levels of the microglial marker Iba1 compared to PCD cells ($p = 0.001$; Fig. 2F).

Regarding phagocytosis, PCD BMDML cells internalised significantly fewer fluorescent microspheres compared to WT cells, ($p = 0.009$; Fig. 2I), indicating reduced phagocytic capacity. To determine whether this difference was influenced by cell size, microsphere uptake was normalised to the cell area. The results remained significant ($p = 0.005$; Fig. 2J), confirming that WT BMDML cells exhibit a higher phagocytic capacity independent of cell size.

Regarding motility, the results showed that PCD BMDML cells exhibit higher motility compared to WT cells ($p = 0.018$; Fig. 2M), consistent with the gene expression data.

Finally, proliferation analyses indicated that PCD BMDML cells exhibit a higher proliferative capacity than WT cells. Specifically, a greater percentage of Ki67-labelled cells was observed in PCD cultures compared to WT cultures ($p = 0.021$; Fig. 2T). In addition, the alamarBlue assays showed that although cell numbers were initially comparable between WT and PCD cultures on day 1, PCD cultures showed increased proliferation over time (days 3, 6, and 9), resulting in a higher overall cell count ($p = 0.001$; Fig. 2U).

In summary, in the absence of the influence of a neural environment, PCD microglia present reduced phagocytic capacity and high motility and proliferation. To verify that the effect was strictly due to the mutation, we performed the same experiments using medium obtained from PCD mouse cultures as a means of differentiating microglia and observed the same behaviour of PCD microglia compared to WT (see Supplementary Fig. S2). Therefore, these findings support a direct role of the *Ccp1* gene in regulating normal microglial function.

3.3. Microglial cells isolated from the cerebral cortex of neonatal PCD mice exhibit altered protein expression and increased phagocytic capacity and motility

After analysing BMDML cells, we next examined genuine microglial cells, those isolated directly from neural tissue that are free from the influence of neuronal death. To this end, we compared microglial cells isolated from the cerebral cortex of neonatal WT and PCD mice. The microglial identity of cortical isolates was further validated by qPCR analysis of general microglial markers, with results consistent with those described below (Supplementary Fig. S3).

Immunohistochemical analysis revealed no significant morphological differences between WT and PCD cells (ameboid, $p = 0.885$; one branch, $p = 0.564$; two branches, $p = 0.561$; three or more branches, $p = 0.885$; Fig. 3C). Similarly, the area of microglial cells isolated from the cerebral cortex did not differ between both experimental groups ($p = 0.463$; Fig. 3D). In contrast, Iba1 expression intensity was higher in microglia from WT mice compared to those from PCD mice ($p = 0.0286$; Fig. 3E).

Additionally, microglia isolated from the cerebral cortex of neonatal

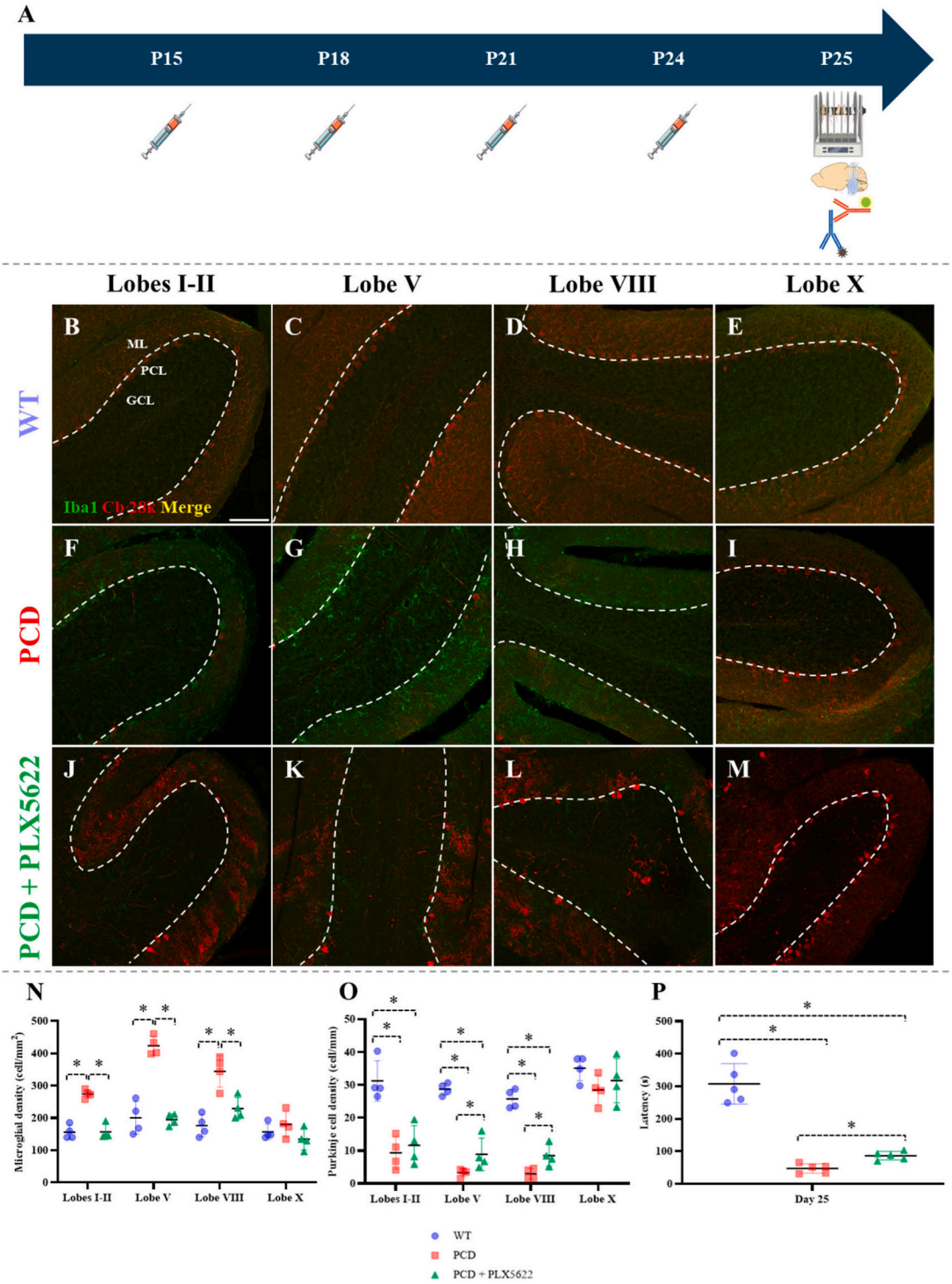

Fig. 1. Effect of eliminating cerebellar microglia using PLX5622. (A) Experimental timeline indicating PLX5622 administration in PCD mice (syringe icon), the day of motor performance assessment (rotarod icon), and the day of sacrifice for immunohistochemical processing (brain and antibody icons). (B–M) Representative sections of the cerebellar vermis from WT, PCD, and PLX5622-treated PCD mice immunolabeled for Iba1 (green) and Calbindin D-28 k (red), organized by cerebellar lobes: (B, F, J) correspond to lobes I–II, (C, G, K) to lobe V, (D, H, L) to lobe VIII, and (E, I, M) to lobe X. Note that untreated PCD mice present a wider staining for microglia and fewer Purkinje cells than WT animals, which is prevented by PLX5622 administration. (N) Quantification of microglial density in the cerebellum of WT, PCD, and PLX5622-treated PCD mice; PCD mice show increased microglial density compared to WT and PLX5622-treated PCD mice, with the latter two groups displaying comparable values. (O) Quantification of Purkinje cell density; PLX5622-treated PCD mice exhibit an intermediate number of Purkinje cells relative to WT and untreated PCD mice. Note that tendencies of both microglial (N) and Purkinje cell densities (O) do not affect lobe X. (P) Rotarod performance at P25; WT mice show a significantly longer latency to fall, and PLX5622-treated PCD mice perform the task better than untreated PCD mice. GCL, granule cell layer; ML, molecular layer; PCL, Purkinje cell layer. Data are shown as the mean ± SD, where each point corresponds to one animal (n = 4-5 animals per group). The central black line indicates the mean and error bars represent the SD. *$p < 0.05$. Scale bar: 100 μm.

PCD mice exhibited higher phagocytic capacity than WT cells, as evidenced by increased uptake of fluorescent microspheres ($p = 0.029$; Fig. 3H). Considering the cell area, significant differences were found between the two experimental groups, with PCD microglia displaying higher values ($p = 0.029$; Fig. 3I). As before, cell size did not interfere with phagocytosis.

Time-lapse video analysis revealed that cortical microglia from PCD mice exhibited higher motility compared to WT microglia ($p = 0.024$; Fig. 3L).

Proliferation analysis showed no differences between PCD and WT cortical microglia. Both groups displayed similar percentages of Ki67-labelled cells ($p = 0.386$; Fig. 3S). Similarly, alamarBlue assays

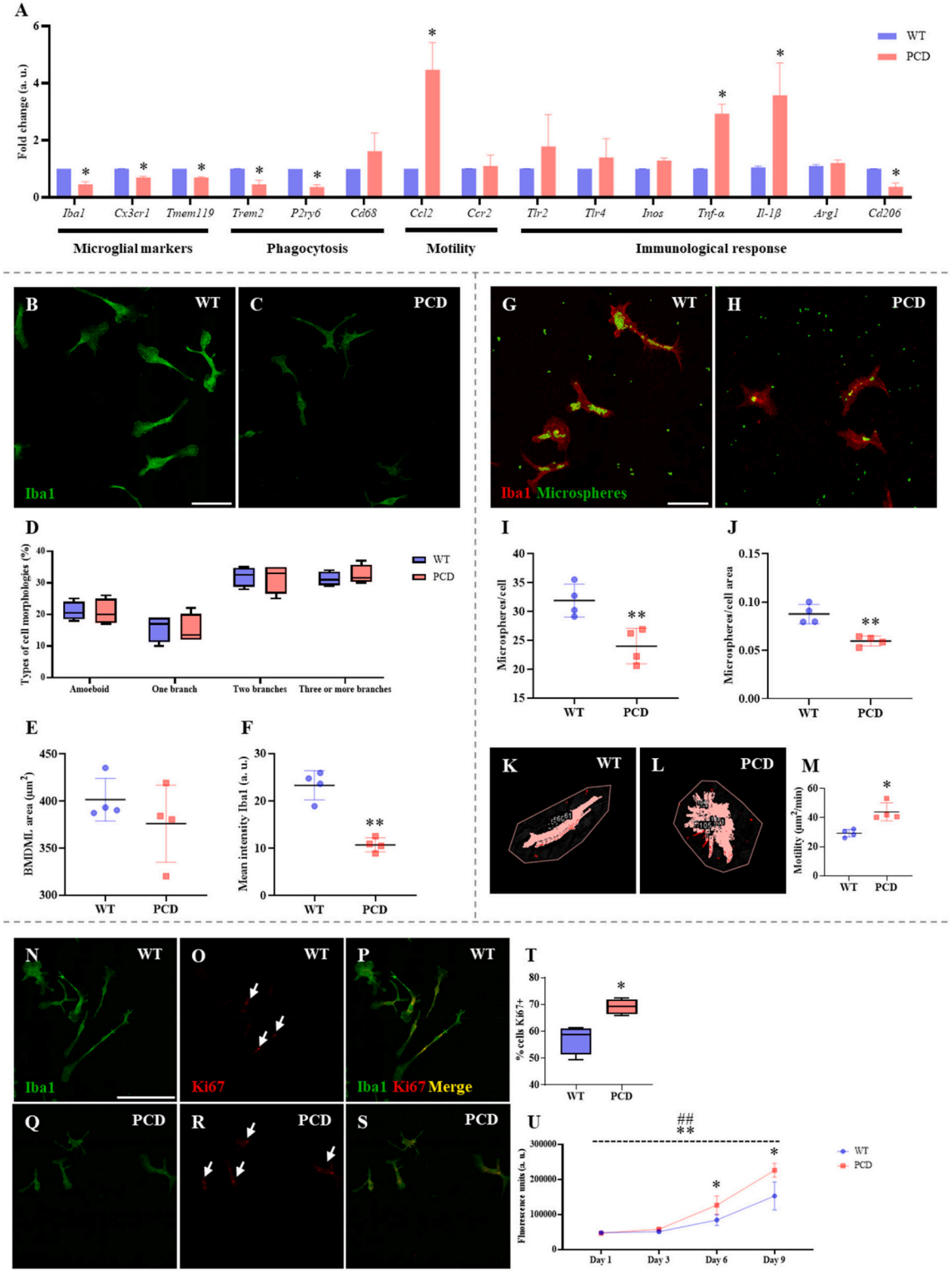

(caption on next page)

Fig. 2. Analysis of WT and PCD BMDML cells. (A) Gene expression analysis of general microglial markers (*Iba1*, *Cx3cr1*, *Tmem119*), phagocytic capacity (*Trem2*, *P2ry6*, *Cd68*), motility (*Ccl2*, *Ccr2*), and innate (*Tlr2*, *Tlr4*), pro-inflammatory (*Inos*, *Tnf-α*, *Il-1β*) and anti-inflammatory (*Arg1*, *Cd206*) immune responses. (B-F) Immunocytochemical analysis. (B, C) Images of BMDML cells labelled with Iba1 antibody (green). (D) Morphologies observed in the cultures and their relative frequencies. Similar percentages of each morphology were observed between the two genotypes. (E) Cell area analysis shows that WT cells have similar areas to PCD cells. (F) Analysis of the intensity of Iba1 expression showing a greater intensity of labelling in WT cells compared to PCD cells. (G-J) Analysis of phagocytic capacity. (G, H) Images of BMDML cells labelled with the Iba1 antibody (red) showing microspheres (green) both inside and outside the cells. (I) WT BMDML cells phagocytosed a greater number of microspheres than PCD BMDML cells. (J) When the area of each cell is considered, it is also observed that WT BMDML cells phagocytose more microspheres than PCD BMDML cells, irrespective of their dimensions. (K-M) Motility analysis of BMDML cells. (K, L) Schematic showing the movement of BMDML WT cells and BMDML PCD cells during time-lapse videos. (M) Quantification of motility showing that WT cells show less motility capacity compared to PCD cells. (N-U) Proliferation analysis. (N-S) Images of WT and PCD BMDMLs labelled with Iba1 antibody (green) and Ki67 antibody (red). (T) A higher percentage of cells expressing Ki67 were found in PCD cell cultures than in WT cell cultures. (U) Analysis of proliferation with alamarBlue over time. The proliferation of PCD cells is higher than in the WT, which is evident from day 3 onwards. Data are shown as the mean ± SD, where each point corresponds to one biological replicate (average of 10 cells per animal; n = 4 animals per group). For boxplots and alamarBlue assays, the single data point shown represents the mean value calculated from all animals in the group (n = 4 animals). *$p < 0.05$, **$p < 0.01$, for overall comparison between genotypes; ##$p < 0.01$, for overall comparison between times. Scale bars: 100 μm.

showed parallel patterns of cell number fluctuations over time in both culture types. However, differences were found between the two experimental groups at day 6 ($p = 0.021$; Fig. 3T), when cell numbers declined rather than increased. This suggests that the observed difference may be due to increased cell death in WT cultures rather than enhanced proliferation in PCD cultures.

In summary, the physiological neural environment influences certain characteristics of PCD microglia: it increases their phagocytic capacity and appears to suppress their proliferation. These findings indicate that the neural environment itself plays a role in modulating—and potentially reversing—certain microglial functions with altered *Ccp1* gene.

3.4. Microglial cells isolated from the cerebellum and olfactory bulb of adult PCD mice exhibit an inflammatory morphology, altered protein expression, and increased phagocytic capacity and cell motility

After analysing the intrinsic effects of *Ccp1* gene deficiency on microglia function, we next sought to investigate how a neurodegenerative environment further influences these cells. For this purpose, we conducted *in vitro* analyses of microglia isolated from the cerebellum and OB, allowing us to compare the impact of two distinct severities of neurodegeneration.

First, morphological differences were observed between experimental groups in microglia isolated from both the cerebellum and OB. Specifically, microglial cells isolated from PCD mice in both regions showed a higher proportion of amoeboid cells, along with a reduced proportion of microglia bearing one or two branches. No significant differences were found in the proportion of cells with three or more branches (cerebellum, amoeboid, $p = 0.020$; one branch, $p = 0.029$; two branches, $p = 0.019$; three or more branches, $p = 0.462$; Fig. 4G / OB, amoeboid, $p = 0.020$; one branch, $p = 0.020$; two branches, $p = 0.020$; three or more branches, $p = 0.695$; Fig. 5G). Thus, we can conclude that microglia isolated from both the cerebellum and OB of PCD animals tend to adopt a more amoeboid shape. Moreover, microglia cells from PCD mice were larger than those of WT mice in both cases (cerebellum; $p = 0.028$; Fig. 4H / OB; $p = 0.007$; Fig. 5H). In line with this, Iba1 expression intensity was higher in microglial cells isolated from the cerebellum and OB of PCD mice compared to those isolated from WT mice (cerebellum, $p = 0.03$; Fig. 4I / OB, $p = 0.001$; Fig. 5I).

Analysis of the phagocytic capacity revealed that microglial cells isolated from PCD mice— whether cerebellum or OB—phagocytosed more neuronal debris than microglia isolated from WT mice (cerebellum, $p = 0.029$; Fig. 4J / OB, $p = 0.013$; Fig. 5J). By contrast, when phagocytosis was normalised to the cell area, no differences were found between the groups (cerebellum, $p = 0.400$; Fig. 4K / OB, $p = 0.500$; Fig. 5K).

These findings suggest that in contrast to microglia from non-degenerative regions (e.g., bone marrow or cerebral cortex) cell size may influence the phagocytic capacity of microglia isolated from neurodegenerative environments such as the cerebellum and OB.

Finally, microglia from PCD mice exhibited higher motility than WT microglia in both regions analysed (cerebellum; $p = 0.025$; Fig. 4N / OB; $p = 0.004$; Fig. 5N).

In conclusion, a pathological environment further alters PCD microglia: it promotes increased proliferation, a shift toward an amoeboid and hyper-ramified morphology, and markedly increases Iba1 expression. Thus, a neurodegenerative environment is necessary for microglia with *Ccp1* deficiency to fully activate some of their main functions.

3.5. Microglia in the cerebellum and olfactory bulb of PCD mice exhibit gene expression characteristic of microglial activation

Our final objective was to analyse microglia in PCD mice *in vivo* to assess the direct influence of neuronal death and to characterise the temporal dynamics of this influence—specifically, before, during, and after the peak of neurodegeneration.

Gene analyses conducted prior to the onset of neurodegeneration in the cerebellum showed elevated expression of several genes in PCD mice compared to the WT control. These included general microglial markers (*Iba1*, *Cx3cr1*), phagocytosis-related genes (*Trem2*, *Dap12*, *P2ry6*), genes associated with motility (*Ccl2*), and inflammatory response (*Tnf-α*, *Il-1β*, *Arg1*; Fig. 6). Similarly, in the OB, higher expression of genes related to motility (*Ccl2*) and immune response (*Tlr2*, *Tnf-α*, *Il1-β*) was found in the PCD mutant compared to WT mice (Fig. 6). Therefore, even before the onset of neurodegenerative processes, microglia in the cerebellum and OB of PCD mice acquire a pre-activated state, with greater activation observed in the cerebellum.

Gene expression analysis during the neurodegenerative phase showed a marked upregulation of nearly all analysed genes in the cerebellum of PCD mice, except for *Inos* (Fig. 6). Similarly, in the OB, PCD mice also exhibited increased expression of most genes, except for *Cd200r* and *Inos* (Fig. 6). These results indicate that during neurodegeneration in PCD mice, genes involved in phagocytosis, motility, and immune response are highly expressed. Thus, in PCD mice both cerebellar and OB microglia are highly activated during neurodegeneration, especially in the cerebellum.

Following the completion of neurodegenerative processes, the cerebellum of PCD mice still showed increased expression of genes corresponding to general markers of microglia (*Cx3cr1*), phagocytosis (*Trem2*, *Dap12*), motility (*Ccl2*, *Ccr2*), and immune response (*Tlr2*, *Tnf-α*; Fig. 6). Thus, once Purkinje cell death had concluded, the exacerbated state of cerebellar microgliosis decreased, presenting more moderate activation levels. By contrast, microglia in the OB of PCD mice maintained high expression levels of nearly all analysed genes, except for *Cd200r*, *Tlr4*, and *Inos* (Fig. 6). Despite the completion of mitral cell death, microglia in the OB of PCD mice continued to express high levels of genes consistent with a state of high activation.

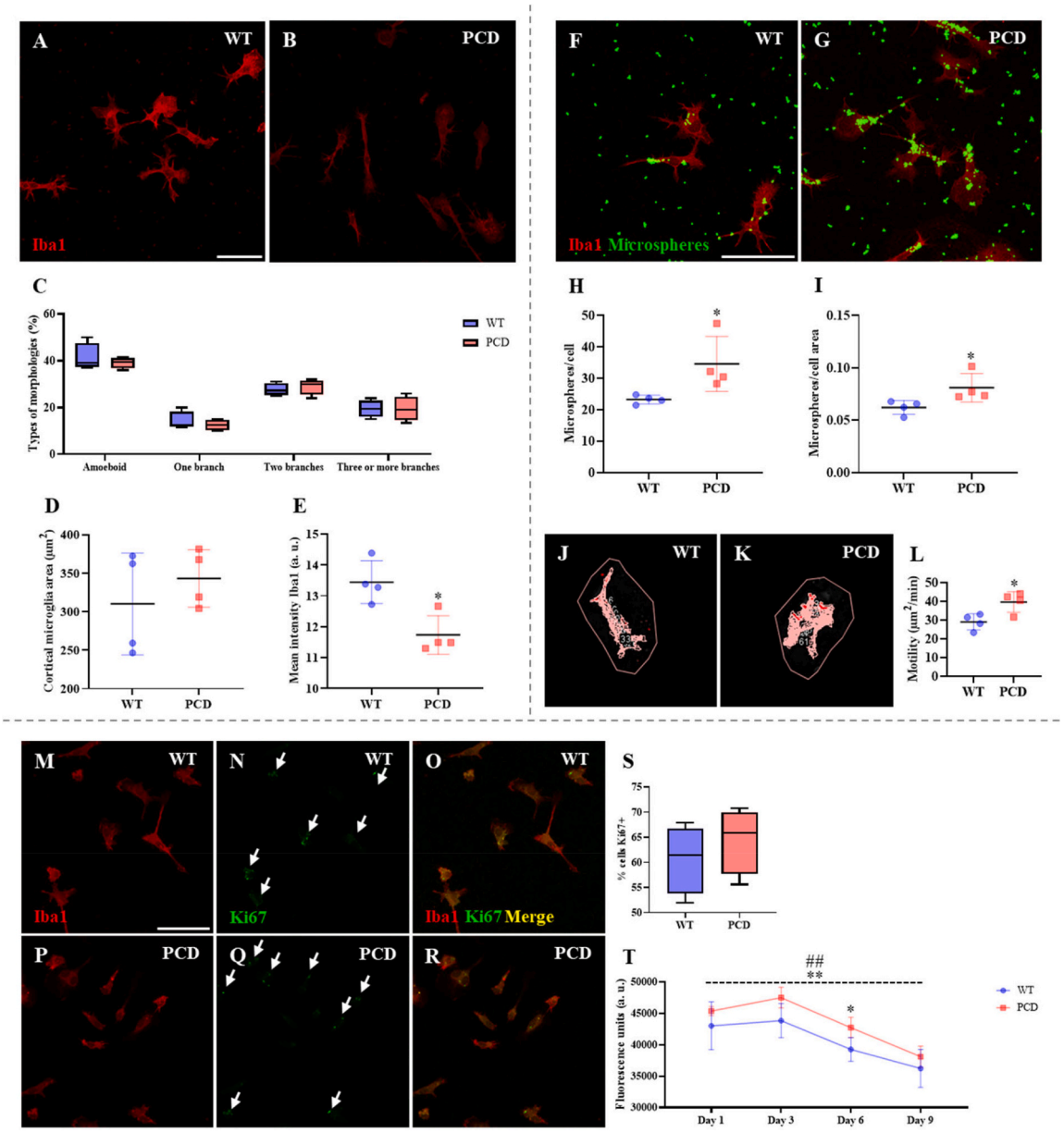

Fig. 3. Analysis of microglia isolated from the cerebral cortex of WT and PCD mice. (A-E) Immunocytochemical analysis of cortical microglia. (A, B) Images of WT and PCD microglial cells labelled with the Iba1 antibody (red). (C) Morphologies observed in the cortical microglia cultures and their relative frequencies. Similar percentages of each morphology were observed between the two genotypes. (D) Cellular area analysis of cortical microglia showing that both WT and PCD cells have similar areas. (E) Analysis of Iba1 intensity in cortical microglia cells showing more intense labelling in WT cells compared to PCD cells. (F-I) Analysis of the phagocytic capacity of cortical microglia. (F, G) Images of cortical microglia isolated from WT and PCD mice labelled with the Iba1 antibody (red) showing microspheres (green) both inside and outside the cells. (H) PCD cortical microglial cells phagocytosed more microspheres than WT cells. (I) When the area of each cell is considered, PCD cells also phagocytosed more microspheres than WT cells, regardless of their size. (J-L) Motility analysis of cortical microglia. (J, K) Schematic showing the movement of WT cells and PCD cells during time-lapse videos. (L) Motility quantification showing that WT cells are less motile compared to PCD cells. (M-T) Proliferation analysis. (M-R) Images of cortical microglia isolated from WT and PCD mice labelled with Iba1 (red) and Ki67 antibodies (green). (S) Chart showing a similar percentage of cortical microglial cells expressing Ki67 in both genotypes. (T) AlamarBlue proliferation analysis of WT and PCD cortical microglia cells over time. Overall, PCD cells were more numerous than WT cells. Data are shown as the mean ± SD, where each point corresponds to one biological replicate (average of 10 cells per animal; n = 4 animals per group). For boxplots and alamarBlue assays, the single data point shown represents the mean value calculated from all animals in the group (n = 4 animals). *$p < 0.05$; **$p < 0.01$, for overall comparison between genotypes; ##$p < 0.01$, for overall comparison between times. Scale bars: 100 µm.

3.6. Microglia in the cerebellum and olfactory bulb of PCD mice exhibit a high density and are distributed towards areas of neurodegeneration

Following gene expression analyses, immunohistochemical techniques were performed to examine the spatial distribution and density of microglia in the cerebellum and OB of PCD mice throughout neurodegeneration.

Prior to the onset of neurodegeneration, microglial density and distribution patterns were comparable between WT and PCD mice in both brain regions. Microglia were distributed homogeneously across the different cerebellar and bulbar layers (Figs. 7 and 8).

However, during peak neurodegeneration, differences emerged between the experimental groups. In the cerebellar vermis of PCD mice (lobes I-II, V, and VIII), a marked increase in microglia density was

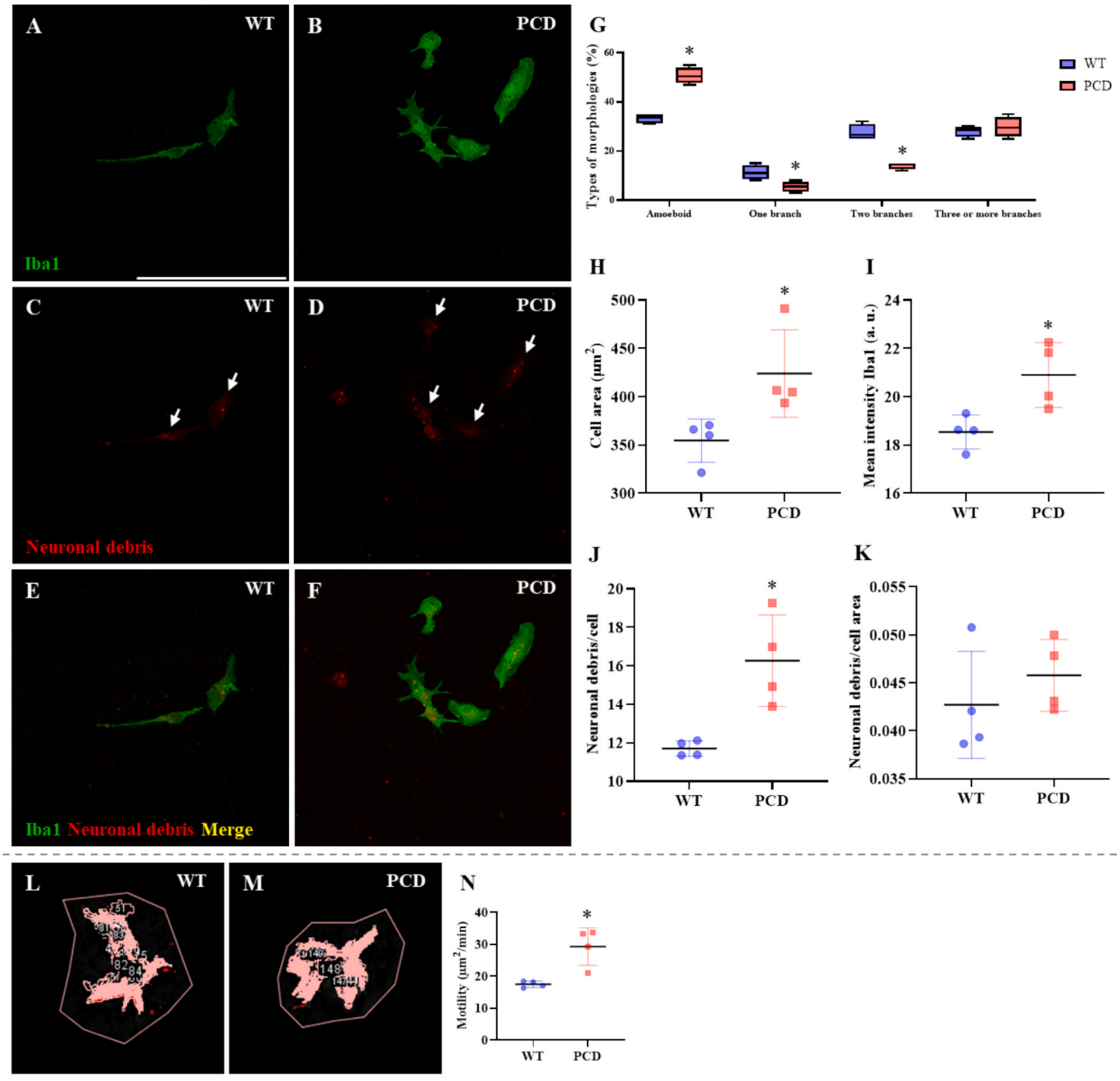

Fig. 4. Analysis of microglia isolated from the cerebellum of WT and PCD mice. (A-K) Immunocytochemical analysis and phagocytic capacity of microglia. (A, B) Images of WT and PCD microglia cells labelled with the Iba1 antibody (green). (G) Morphologies observed in WT and PCD cerebellar microglia cultures and their relative frequencies. Microglia isolated from the cerebellum in both experimental groups had a high percentage of amoeboid cells, notably higher in microglial cells from the cerebellum of PCD mice. Regarding branching morphologies, only the percentages of cells with three or more branches were similar between the two experimental groups. (H) Cell area analysis of microglia showing that the area of PCD cells is larger than the area of WT cells. (I) Analysis of Iba1 expression showing a higher intensity of labelling in PCD microglia compared to WT cells. (C-F) Images of neuronal debris (red) and WT and PCD microglial cells labelled with Iba1 (green) showing these neuronal debris both inside and outside the cells. The arrows correspond to the neuronal debris inside the cells. (J) PCD microglia phagocytosed more neuronal debris than WT microglia. (K) When relating phagocytosis to the area of each cell, no significant differences were found; therefore, cell size may influence phagocytic activity. (L-N) Motility analysis. (L, M) Schematic showing the movement of WT cells and PCD cells during time-lapse videos. (N) Motility quantification showing that PCD cells are more mobile than WT microglia. Data are shown as the mean ± SD, where each point corresponds to one biological replicate (average of 10 cells per animal; n = 4 animals per group). *$p < 0.05$. Scale bar: 100 µm.

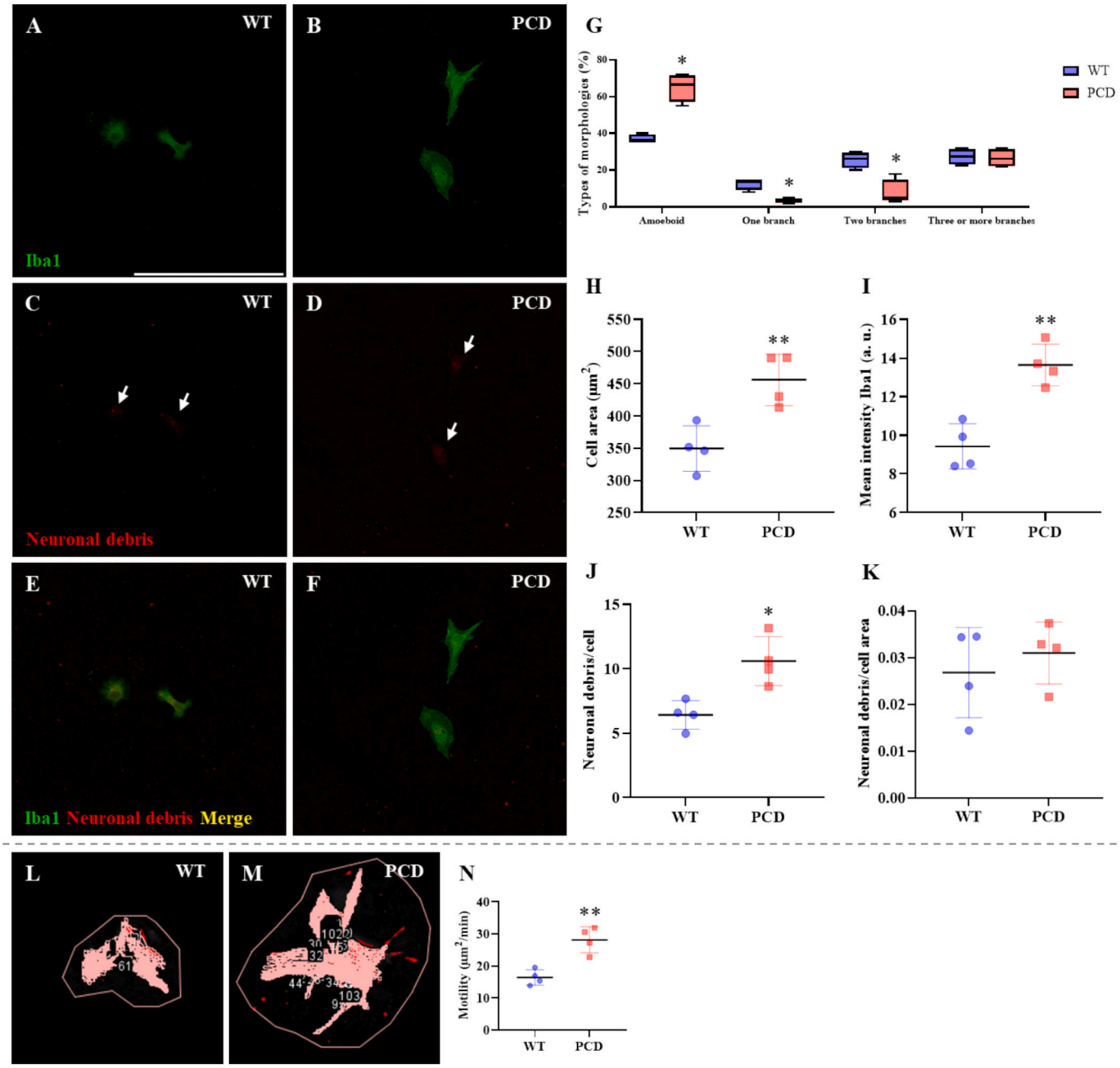

Fig. 5. Analysis of microglia isolated from the OB of WT and PCD mice. (A-K) Immunocytochemical and phagocytic capacity analysis of microglia. (A, B) Images of WT and PCD microglia cells labelled with the Iba1 antibody (green). (G) Morphologies observed in WT and PCD microglia cultures and their relative frequencies. More amoeboid cells were observed in PCD cultures compared to WT cultures. In contrast, cells with one or two branches were more abundant in WT cultures. Regarding cells with three or more branches, similar values were found in both cultures. (H) Cell area analysis of microglia showing that the area of PCD cells is larger than that of WT cells. (I) Analysis of Iba1 expression showing a higher intensity of labelling in PCD microglial cells compared to WT cells. (C-F) Images of neuronal debris (red) and WT and PCD microglial cells labelled with Iba1 (green) showing these neuronal debris both inside and outside the cells. The arrows correspond to the neuronal debris inside the cells. (J) PCD microglial cells phagocytosed more neuronal debris than WT cells. (K) When relating phagocytosis to the area of each cell, no significant differences were found, so cell size may affect phagocytic activity. (L-N) Motility analysis. (L, M) Schematic showing the movement of WT cells and PCD cells during time-lapse videos. (N) Motility quantification showing that PCD cells are more mobile than WT microglia. Data are shown as the mean ± SD, where each point corresponds to one biological replicate (average of 10 cells per animal; n = 4 animals per group). *$p < 0.05$; **$p < 0.01$. Scale bar 100 µm.

observed, especially within the molecular and Purkinje cell layers. However, in lobe X, similar values were found in both genotypes (Fig. 7), consistent with its known neuroprotective properties (see Discussion). In the OB of PCD mice, microglia density also increased, particularly around the mitral cell layer (Fig. 8). Moreover, the changes in distribution and density were more pronounced in the cerebellum than in the OB.

Once the neurodegenerative processes were over, both the cerebellum and OB of PCD mice retained microglial density and distribution patterns like those observed during peak degeneration (Figs. 7 and 8). In the cerebellum, however, an additional increase in microglial density was detected in the granule cell layer (Fig. 7). This redistribution likely reflects the completion of Purkinje cell death, prompting microglia that had previously migrated and proliferated in the mitral cell and Purkinje

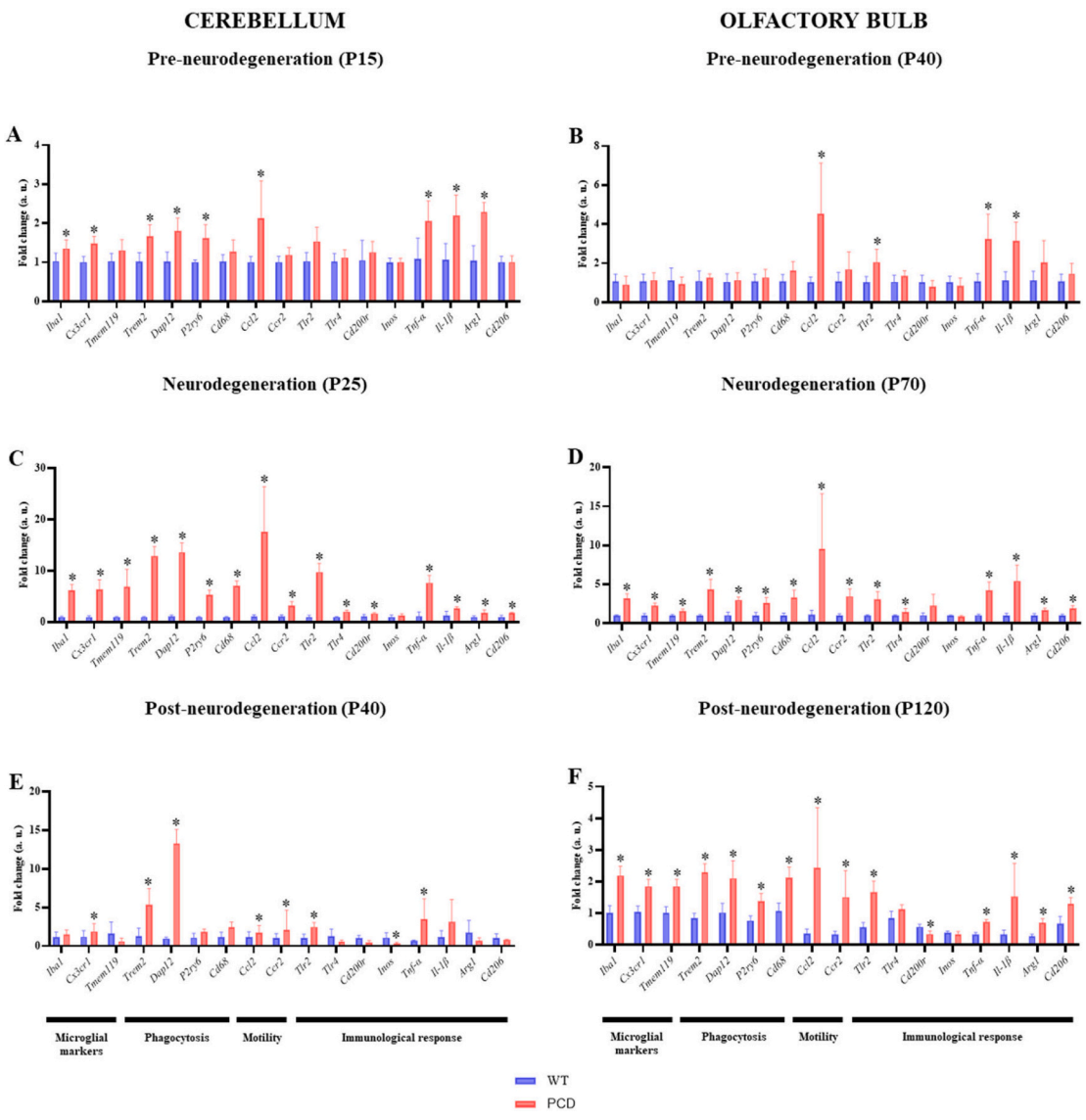

Fig. 6. Gene expression analysis in the cerebellum and OB of WT and PCD mice. General markers of microglia (*Iba1*, *Cx3cr1*, *Tmem119*), phagocytic capacity (*Trem2*, *Dap12*, *P2ry6, Cd68*), motility (*Ccr2*, *Ccl2*), and innate (*Tlr2*, *Tlr4*, *Cd200r*), pro-inflammatory (*Inos*, *Tnf-α*, *Il-1β*) and anti-inflammatory (*Arg1*, *Cd206*) immune responses were analysed before, during, and after neurodegenerative processes. (A) Gene expression analysis in the cerebellum of WT and PCD mice at postnatal age P15, before the onset of Purkinje cell death. Higher expression of *Iba1, Cx3cr1*, *Trem2*, *Dap12*, *P2ry6*, *Ccl2*, *Tnf-α, Il-1β*, and *Arg1* was found in PCD mice compared to WT mice. (B) Gene expression analysis in the OB of WT and PCD mice at P40, before the onset of mitral cell death. Increased expression of *Ccl2*, *Tlr2*, *Tnf-α*, and *Il-1β* was found in PCD mice compared to WT mice. (C) Gene expression analysis in the cerebellum of WT and PCD mice at P25, during peak Purkinje cell degeneration. Increased gene expression was observed in virtually all genes analysed: *Iba1*, *Cx3cr1*, *Tmem119*, *Trem2*, *Dap12*, *P2ry6*, *Cd68*, *Ccl2*, *Ccr2*, *Tlr2*, *Tlr4*, *Cd200r*, *Tnf-α*, *Il-1β*, *Arg1*, and *Cd206*, except for *Inos*. (D) Gene expression analysis in the OB of WT and PCD mice at P70, during peak mitral cell degeneration. Significant differences were found in the expression of nearly all genes analysed: *Iba1*, *Cx3cr1*, *Tmem119*, *Trem2*, *Dap12*, *P2ry6*, *Cd68*, *Ccl2*, *Ccr2*, *Tlr2*, *Tlr4*, *Tnf-α*, *Il-1β*, *Arg1*, and *Cd206*, except for *Cd200r* and *Inos*. (E) Gene expression analysis in the cerebellum of WT and PCD mice at P40, after Purkinje cell death. PCD mice were found to have increased expression of *Cx3cr1*, *Trem2*, *Dap12*, *Ccl2*, *Ccr2*, *Tlr2*, and *Tnf-α* and reduced expression of *Inos*. (F) Gene expression analysis in the OB of WT and PCD mice at P120, after mitral cell death. Significantly increased expression continued to be observed in almost all genes analysed: *Iba1*, *Cx3cr1*, *Tmem119*, *Trem2*, *Dap12*, *P2ry6*, *Cd68*, *Ccl2*, *Ccr2*, *Tlr2*, *Tnf-α*, *Il-1β*, *Arg1*, and *Cd206*. Data are shown as the mean ± SD, calculated from four animals per group (n = 4). *$p < 0.05$.

cell layers to return to their former location in the granule cell layer. In the case of the OB, the density and distribution of microglial cells were identical to what was observed at the previous time point (Fig. 8).

3.7. During and after neurodegenerative processes, microglia in the cerebellum and olfactory bulb of PCD mice exhibit a morphology characteristic of activated microglial states

In addition to distribution, the morphology of microglia in the cerebellum and OB of PCD mice was also analysed.

Prior to the onset of neurodegenerative processes, microglia in both regions exhibited similar morphologies in the two genotypes. Cells had a small cell body and numerous thin, branched processes, and a large concentric surveillance area—characteristics of a resting state (Vidal-Itriago et al., 2022). Nevertheless, qualitative *in vivo* analysis revealed subtle early morphological alterations in PCD microglia, specifically at P15 in the cerebellum and P40 in the OB, prior to overt neuronal degeneration. Although these changes were modest and not subjected to

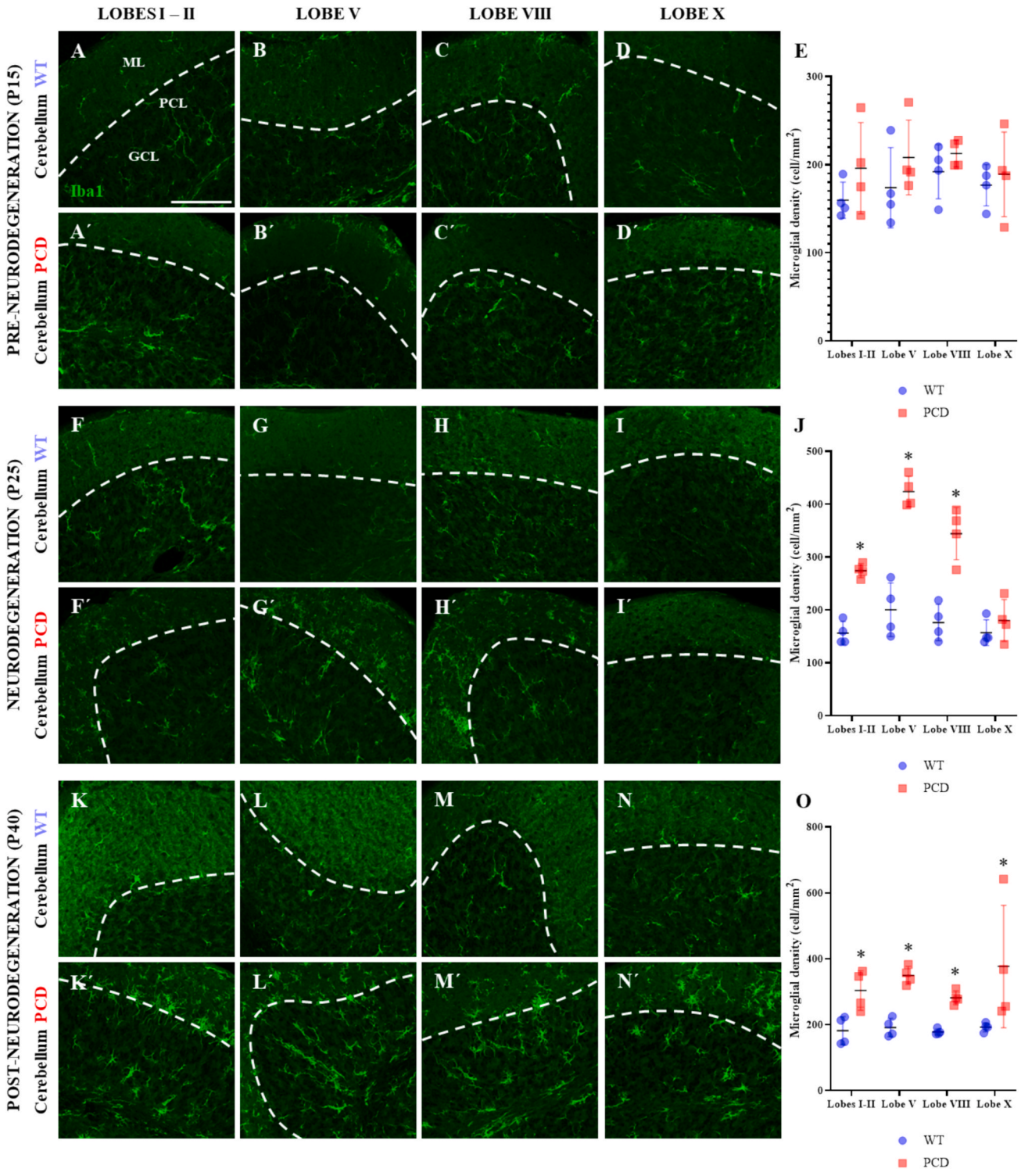

Fig. 7. Analysis of the distribution and density of microglia in the cerebellar cortex of WT and PCD mice. Images of the different cerebellar lobes analysed (lobes I-II, V, VIII, and X) show Iba1-labelled microglia (green) distributed throughout the different layers of the cerebellar cortex. The dotted line delimits the Purkinje cell layer, orienting the molecular layer above it and the granule cell layer below it. (A-D, Á-Ď) Histological sections showing microglia in the cerebellum of WT and PCD mice at P15. Homogeneous distribution patterns were observed in both genotypes. (E) Analysis of microglia density in the cerebellum of WT and PCD mice at P15; no differences were observed between genotypes. (F-I, F́-Í) Histological sections showing microglia in the cerebellum of WT and PCD mice at P25. Note that at this age cerebellar degeneration in PCD mice results in marked microgliosis directed towards the molecular layer and Purkinje cell layer in all cerebellar lobes except lobe X. (J) Analysis of microglial density in the cerebellum of WT and PCD mice at P25 confirms the above-mentioned microgliosis in PCD mice. (K-N, Ḱ-Ń) Histological sections showing the microglia in the cerebellum of WT and PCD mice at P40. The differences found at P25 are maintained, while microgliosis is detected in lobe X in PCD mice. (O) Analysis of microglia density in the cerebellum of WT and PCD mice at P40; PCD mice present higher densities in all analysed lobes. GCL, granule cell layer; ML, molecular layer; PCL, Purkinje cell layer. Data are shown as the mean ± SD, where each point corresponds to one animal (n = 4 animals per group). The central black line indicates the mean and error bars represent the SD. *$p < 0.05$. Scale bar: 200 μm.

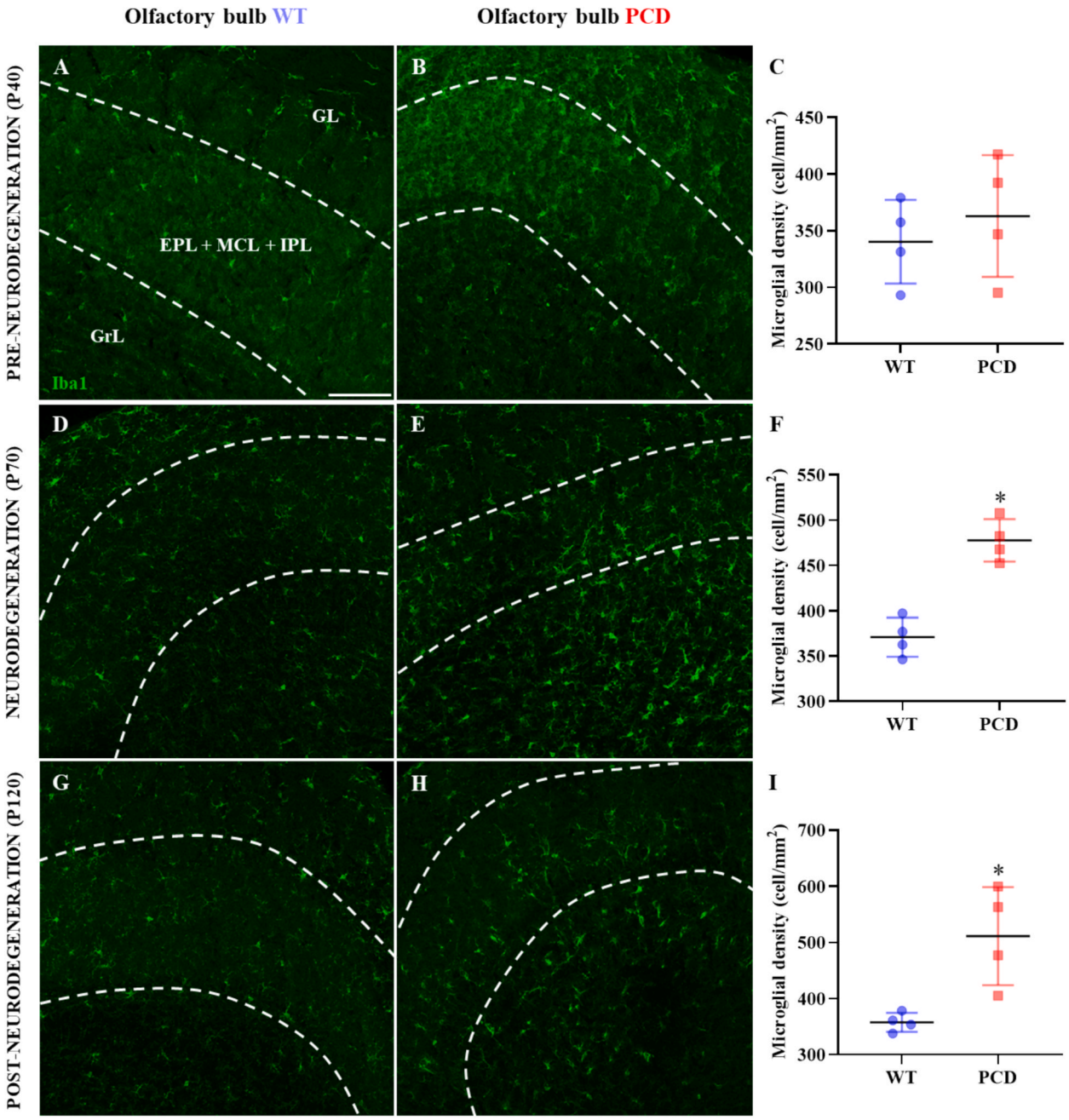

Fig. 8. Analysis of the distribution and density of microglia in the OB of WT and PCD mice. The images show Iba1-labelled microglial cells (green) distributed throughout the different layers of the OB. The dotted lines delimit the division between the three regions studied. The orientation of the images shows the glomerular layer at the top, the mitral and perimitral layers in the middle, and the granule cell layer at the bottom. (A, B) Histological sections showing microglia in the OB of WT and PCD mice at P40. Homogeneous distribution patterns were observed in both genotypes. (C) Analysis of microglia density in the OB of WT and PCD mice at P40 showing no differences between genotypes. (D, E) Histological sections showing microglia in the OB of WT and PCD mice at P70. Note that bulbar degeneration of PCD mice results in marked microgliosis directed towards the mitral cell layer. (F) Analysis of microglia density in the OB of WT and PCD mice at P70 confirming microgliosis in mutant mice. (G, H) Histological sections showing microglia in the OB of WT and PCD mice at P120. The differences found at P70 are maintained, with microgliosis directed towards the mitral cell layer. (I) Analysis of microglia density in the OB of WT and PCD mice at P120 still showing a higher density in mutants. EPL, external plexiform layer; GL, glomerular layer; GrL, granule cell layer; IPL, inner plexiform layer; MCL, mitral cell layer. Data are shown as the mean ± SD, where each point corresponds to one animal (n = 4 animals per group). The central black line indicates the mean and error bars represent the SD. *$p < 0.05$. Scale bar: 100 μm.

quantitative morphometric analysis, they suggest an early alteration of microglial structural organisation associated with *Ccp1* deficiency (data not shown).

In contrast, during peak Purkinje cell and mitral cell degeneration, microglia in PCD mice underwent pronounced morphological changes. This included marked hypertrophy of the cell body, increased soma size, and progressive shortening and thickening of processes, resulting in amoeboid and/or hyper-ramified morphologies typical of activated microglia (Vidal-Itriago et al., 2022; Figs. 9 and 10). Representative high-resolution images of microglial morphology in the cerebellum and OB are provided in Supplementary Figs. S4 and S5, respectively. In addition, the microglial surveillance area was significantly reduced, and microglial processes were directed towards Purkinje and mitral cells (Figs. 9 and 10), probably to phagocytize debris and remove it from the

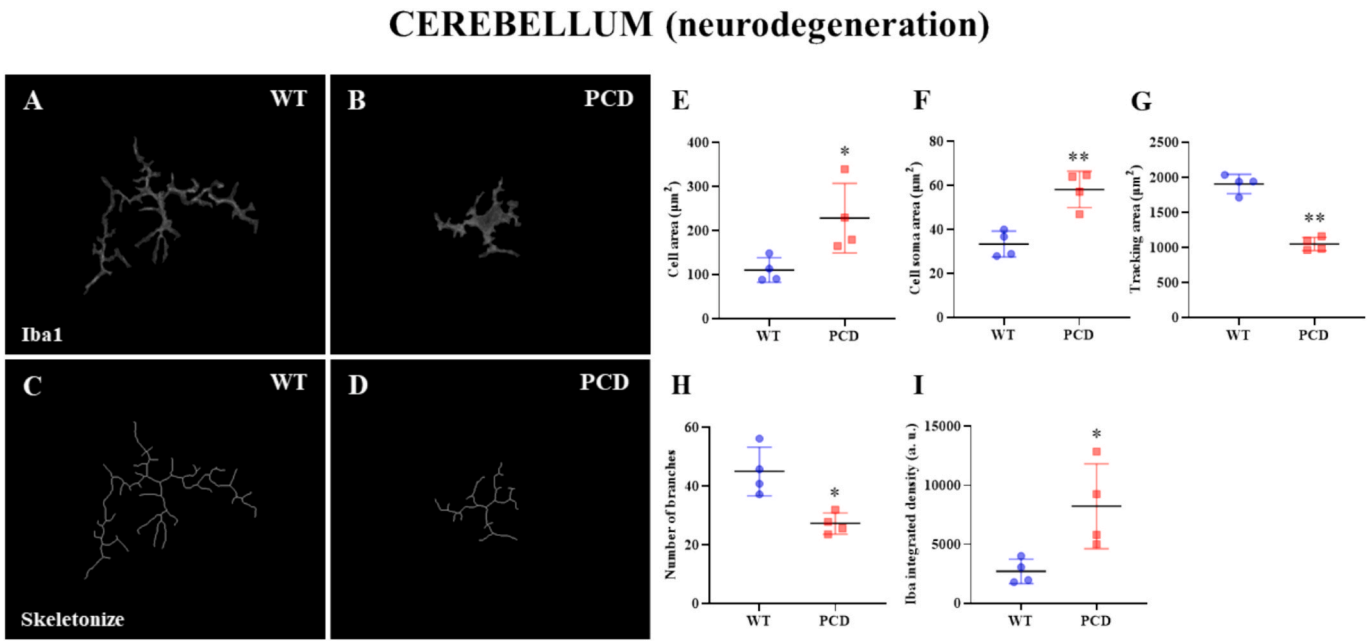

Fig. 9. Morphological analysis of the cerebellar microglia in WT and PCD mice during the neurodegeneration processes. (A-D) Images showing genuine microglial cells labelled with Iba1 (A, B) and their transformation into a schematic image (skeletonize; C, D) for individual analysis. (E-I) Charts showing the results of the cell area, cell soma area, tracking area, branch number, and Iba1 expression analyses. PCD microglia cells exhibit a larger cell area (E), bigger soma (F), smaller homing area (G), reduced number of branches (H), and more intense Iba1 expression (I). Data are shown as the mean ± SD, where each point corresponds to one biological replicate (average of 10 cells per animal; n = 4 animals per group). *$p < 0.05$; **$p < 0.01$. Representative high-resolution images of cerebellar microglia are provided in Supplementary Material S4.

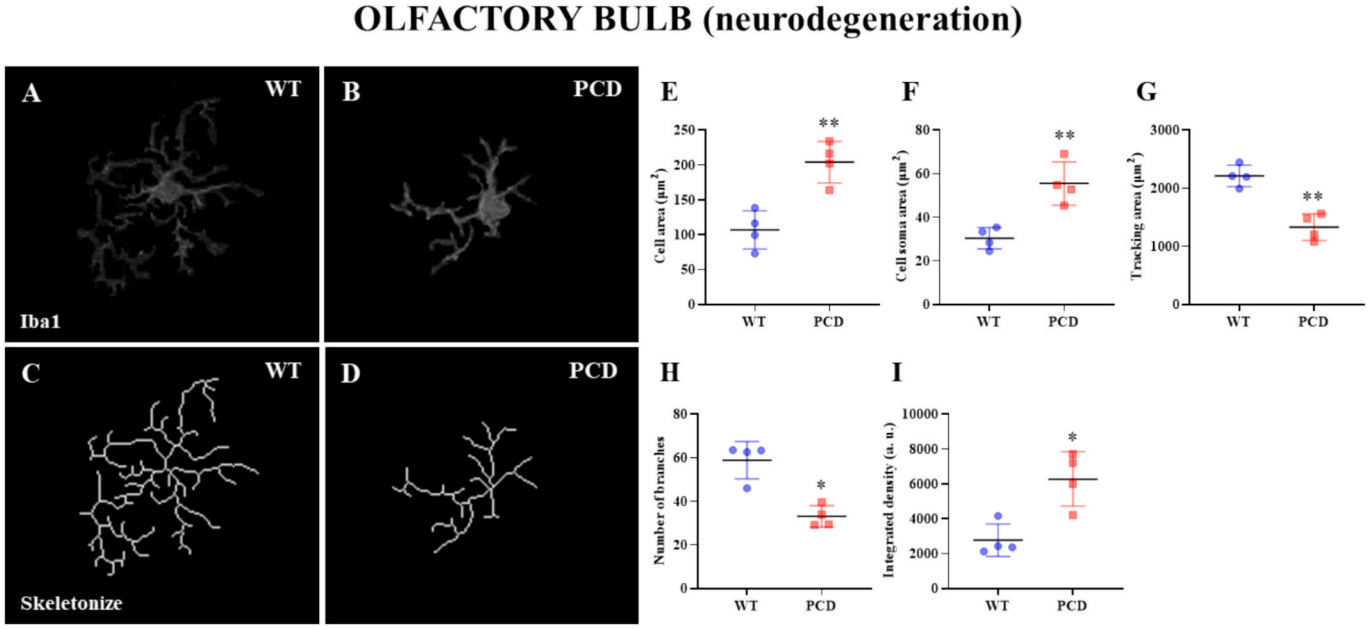

Fig. 10. Morphological analysis of the OB microglia in WT and PCD mice during the neurodegeneration processes. (A-D) Images showing genuine microglial cells labelled with Iba1 (A, B) and their transformation into a schematic image (skeletonize; C, D) for individual analysis. (E-I) Charts showing the results of the cell area, cell soma area, tracking area, branch number, and Iba1 expression analyses. PCD microglia cells exhibit a larger cell area (E), soma bigger (F), smaller homing area (G), reduced number of branches (H), and more intense Iba1 expression (I). Data are shown as the mean ± SD, where each point corresponds to one biological replicate (average of 10 cells per animal; n = 4 animals per group). *$p < 0.05$; **$p < 0.01$. Representative high-resolution images of OB microglia are provided in Supplementary Material S5.

surrounding medium. These changes were more pronounced in cerebellar microglia, suggesting a more intense activation compared to OB microglia.

After the neurodegenerative processes had concluded, microglia in both regions of PCD mice continued to exhibit amoeboid and hyperbranched morphologies, especially in the case of the OB. By contrast, cerebellum microglia began to display more extensively branched morphologies, with elongated processes and smaller bodies—features more typical of resting states (data not shown).

3.8. Microglia in the cerebellum and olfactory bulb of PCD mice showed proinflammatory and anti-inflammatory expression from the onset of neurodegenerative processes

To further characterise the inflammatory nature of microglia in PCD mice, we performed a series of additional immunohistochemical analyses in both the cerebellum and OB using markers associated with microglial functions: CD45 (reactive microglia), CD16/32 (pro-inflammatory activity) and CD206 (anti-inflammatory activity). Since CD45 is expressed to varying degrees by all microglial cells, we quantified its integrated density (i.e. the fluorescence intensity) using the 'Threshold' tool in FIJI. For CD16/32 and CD206, which are selectively expressed under pro- and anti-inflammatory conditions respectively (Pérez-Martín et al., 2023; Del Pilar et al., 2024). We calculated the percentage of Iba1-

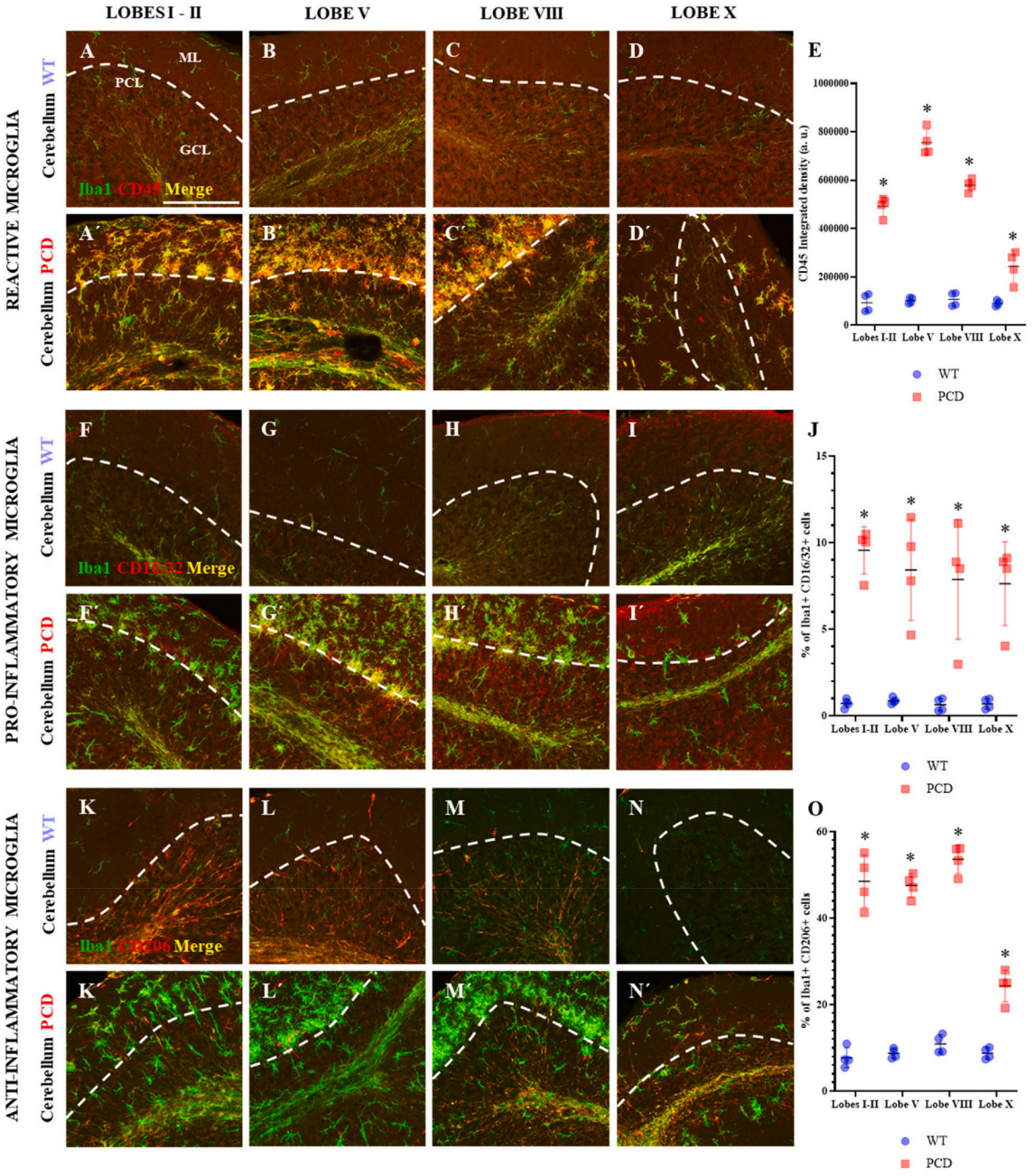

Fig. 11. Analysis of the microglial phenotype in the cerebellar vermis of WT and PCD mice. Sections correspond to cerebellar lobes I-II, V, VIII, and X. Dotted lines delimit the Purkinje cell layer, with the molecular layer situated above the line and the granular layer below it. (A-D, Á-D́) Histological sections showing microglia in the cerebellum of WT and PCD mice labelled with Iba1 (green) and CD45 (reactive microglia, red). (E) Quantitative analyses of the expression of the reactive microglia marker CD45 in the cerebellum at P25. In general, a higher intensity of CD45 expression was observed in the cerebellum of PCD mice. (F- I, F́-Í) Histological sections showing microglia in the cerebellum of WT and PCD mice labelled with Iba1 (green) and CD16/32 (pro-inflammatory microglia, red). (J) Quantitative analysis of the co-expression of Iba1 and CD16/32 markers in the cerebellum at P25. Note that significant co-expression of Iba1 and CD16/32 was only observed in the cerebellum of PCD mice. (K-N, Ḱ-Ń) Histological sections showing microglia in the cerebellum of WT and PCD mice labelled with Iba1 (green) and CD206 (anti-inflammatory microglia, red). (O) Quantitative analysis of the co-expression of Iba1 and CD206 markers in the cerebellum at P25. Co-expression of Iba1 and CD206 was observed mainly in the cerebellum of PCD mice. GCL, granule cell layer; ML, molecular layer; PCL, Purkinje cell layer. Data are shown as the mean ± SD, where each point corresponds to one animal (n = 4 animals per group). The central black line indicates the mean and error bars represent the SD. *$p < 0.05$. Scale bar: 100 μm.

positive cells co-expressing each marker (i.e., double-labelled for Iba1 and CD16/32 or CD206 relative to total Iba1 + cells).

Before the onset of neurodegeneration, expression levels of CD45, CD16/32, and CD206 were slightly elevated in both the cerebellum and OB of PCD mice compared to the WT control (data not shown), with CD206, the anti-inflammatory marker, being the most prominently increased. This possibly reflects the detection of pre-neurodegenerative signals by microglia (see Discussion).

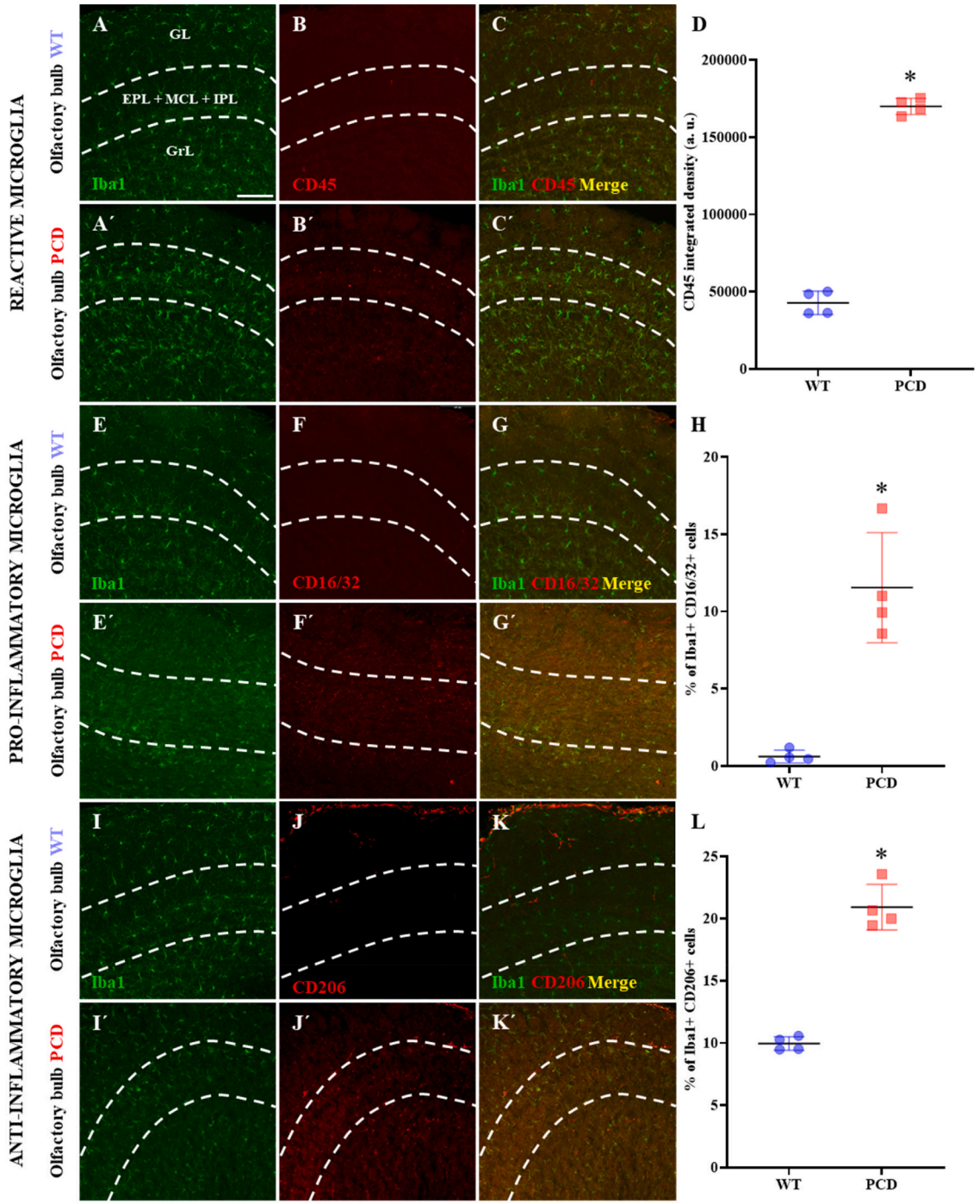

Fig. 12. Analysis of the microglial phenotype in the OB of WT and PCD mice. Dotted lines delineate the division between the three regions studied. The orientation of the images situates the glomerular layer at the top, the mitral and perimitral layers in the centre, and the granule cell layer at the bottom. (A-C, Á-Ć) Histological sections showing microglia in the OB of WT and PCD mice labelled with Iba1 (green) and CD45 (reactive microglia, red). (D) Quantitative analysis of the expression of the reactive microglia marker CD45 in the OB at P70 showing a higher expression in PCD mice compared to WT mice. (E-G, É-Ǵ) Histological sections showing microglia in the OB of WT and PCD mice labelled with Iba1 (green) and CD16/32 (pro-inflammatory microglia, red). (H) Quantitative analysis of the co-expression of Iba1 and CD16/32 markers in the OB at P70. Note that only significant expression of CD16/32 was observed in the microglia of PCD mice. (I- K, Í-Ḱ) Histological sections showing microglia in the OB of WT and PCD mice labelled with Iba1 (green) and CD206 (anti-inflammatory microglia, red). (L) Quantitative analysis of the co-expression of Iba1 and CD206 markers in the OB at P70. Higher CD206 expression is observed in the OB of PCD mice compared to WT mice. EPL, external plexiform layer; GL, glomerular layer; GrL, granule cell layer; IPL, inner plexiform layer; MCL, mitral cell layer. Data are shown as the mean ± SD, where each point corresponds to one animal (n = 4 animals per group). The central black line indicates the mean and error bars represent the SD. *$p < 0.05$. Scale bar: 100 μm.

During peak neurodegeneration, expression of all three markers was markedly increased in both regions of PCD mice, likely as a direct response to Purkinje and mitral cell degeneration. One of the markers showing the strongest expression is CD45, indicating that microglia are in a state of heightened immune reactivity. Additionally, this reactivity is predominantly of an anti-inflammatory nature, as evidenced by the more prominent expression of CD206. This increase was more evident in the cerebellum (Fig. 11) than in the OB (Fig. 12 and Supplementary Fig. S6), consistent with the more aggressive microgliosis observed in the former.

After the neurodegenerative processes were concluded, elevated expression of CD45, CD16/32, and CD206 persisted in both brain regions (data not shown), with CD206 expression being the most sustained, mainly in the OB. This indicates that the anti-inflammatory response is the one that predominantly persists.

In summary, these results show that once neurodegenerative processes begin in PCD mice, a pro- and anti-inflammatory microglial phenotype coexists. These findings are consistent with the results obtained through the gene expression analysis, as microglia in the cerebellum and OB of PCD mice exhibit both pro-inflammatory and anti-inflammatory functions at the same time manifested as a dual response.

4. Discussion

Elimination of microglia from the cerebellum of PCD mice resulted in a significant reduction in Purkinje cell death. Therefore, although microglia are not the sole direct cause of neuronal degeneration, these findings indicate that they actively contribute to disease progression by exacerbating and accelerating neurodegenerative processes, in line with observations in other neurodegenerative disorders (Henry et al., 2020; Stojiljkovic et al., 2022). Importantly, several independent lines of *in vivo* evidence support a functional link between microglial activity and neuronal vulnerability in the PCD model. In the present study, pharmacological reduction of microglial density was accompanied by a marked increase in Purkinje cell survival. In addition, previous work from our laboratory has demonstrated that attenuation of the microglial inflammatory response using anti-inflammatory treatments leads to improved Purkinje cell survival (Pérez-Martín et al., 2023). Moreover, replacement of resident microglia through transplantation of healthy WT bone marrow significantly reduced neuronal loss during the neurodegenerative and inflammatory phase of PCD mice (Díaz et al., 2012), likely by shifting microglia towards a more protective phenotype. Taken together, these converging observations strongly support a causal contribution of microglial activity to Purkinje cell degeneration in this model. To further elucidate the role of microglia in this model, we employed a combination of *in vitro* and *in vivo* approaches to delve deeper into the complexities of microglial functioning.

In *in vitro* experiments, BMDML cells differentiated from PCD mice exhibited reduced expression of general microglial markers compared to their WT counterpart. This observation suggests that the *Ccp1* gene may play a role in the differentiation of BMHSCs into BMDML cells, potentially maintaining them in a more undifferentiated state, with certain stem cell-like features. Supporting this hypothesis, previous studies from our laboratory have shown that mutations in *Ccp1* delay the differentiation and maturation of both Purkinje cells and myeloid cells in PCD mice (Muñoz-Castañeda et al., 2018; Del Pilar et al., 2021). Additionally, other research has shown that CCP1 deficiency is associated with impaired differentiation and the maintenance of pluripotency in embryonic stem cells (Ye et al., 2018). These findings collectively suggest that *Ccp1* may be involved in cell maturation processes, independent of cell type.

Moreover, Iba1 expression was markedly reduced in both BMDML cells and microglia isolated from the cerebral cortex of PCD mice. Previous studies have shown that the cytoplasmic distribution of Iba1 is partially dependent on cytoskeletal dynamics. It is plausible that mutations in the *Ccp1* gene lead to hyperglutamylation of tubulin, resulting in microtubule destabilisation in microglia-like what has been observed in Purkinje cells (Berezniuk et al., 2012; Muñoz-Castañeda et al., 2018). This cytoskeleton disruption could alter the proper localisation and expression of Iba1, resulting in inappropriate levels of this marker. Interestingly, in microglia isolated from the cerebellum and OB during peak periods of neurodegeneration, Iba1 expression was significantly upregulated, most probably in response to neurodegeneration (Michalski et al., 2017; Ousta et al., 2022).

Morphological analysis of cultured cells revealed that BMDML cells and microglia isolated from the cerebral cortex exhibited comparable morphologies between both experimental groups. However, microglia from the cerebellum and OB of PCD mice displayed more amoeboid and/or highly ramified morphologies. Both morphologies could be associated with microglial activation triggered by the degeneration of Purkinje or mitral cells, as observed *in vivo* (see below), and in certain neuropathological conditions (Paasila et al., 2019; Illes et al., 2020; Vidal-Itriago et al., 2022). These findings suggest that mutations in the *Ccp1* gene do not alter the morphology of resting BMDML or microglial cells. However, under conditions of neuronal damage, the size and shape of PCD microglia change and present a clearly activated phenotype (Vidal-Itriago et al., 2022).

The apparent discrepancy between the limited morphological alterations observed *in vitro* under basal conditions and the early changes detected *in vivo* likely reflects the fundamental differences between these experimental contexts. *In vivo*, microglia are embedded within a highly complex and dynamic tissue environment, where neuronal activity, cell–cell interactions, extracellular matrix components, and inflammatory cues (Vidal-Itriago et al., 2022) can amplify subtle cytoskeletal defects associated with *Ccp1* deficiency. In contrast, the reductionist nature of *in vitro* systems may mask early alterations, such that genotype-dependent morphological changes become evident primarily under conditions of neuronal damage or after prior exposure to a degenerative milieu.

In the assessment of the phagocytic capacity of microglial cells, PCD BMDML cells exhibited significantly reduced phagocytic capacity compared with WT BMDML cells. This suggests that mutations in the *Ccp1* gene impair microglia phagocytosis, potentially exacerbating primary neuronal loss in PCD mice due to inefficient clearance of cellular debris (Guo et al., 2019; Beccari et al., 2023). This functional weakening may be influenced by the reduced differentiation of PCD BMDML cells, as insufficient microglial maturation could compromise the development of their functions (Wu et al., 2019). In addition, microtubule destabilisation—previously reported in various cell types in the PCD model (Berezniuk et al., 2012; Muñoz-Castañeda et al., 2018; Franco-Bocanegra et al., 2019; Del Pilar et al., 2021; Ramadan et al., 2021; Möller et al., 2022) —may also affect BMDML cells, negatively influencing the process of phagocytosis. Interestingly, microglial cells isolated from the cerebral cortex, cerebellum, and OB of PCD mice exhibited increased phagocytic activity. This finding suggests that the neuronal environment—even without any overt damage—is responsible for this radical change in the phagocytic capacity of PCD BMDML cells. Moreover, uncontrolled and excessive phagocytosis has been implicated in the exacerbation or even initiation of neuronal cell death (Fu et al., 2014; Herzog et al., 2019; Podleśny-Drabiniok et al., 2020; Wang et al., 2021; Chen et al., 2022). Thus, in the PCD model, heightened microglia phagocytic capacity may contribute to the neuropathological processes observed in the cerebellum and OB. Both regions are characterised by a multitude of nerve connections that are established through pruning by microglia (Lin et al., 2000; Arcuri et al., 2017). Dysregulation of the microglia phagocytic capacity could impair the proper establishment of neuronal connections and synapses, potentially triggering premature neuronal loss, as observed in this model of neurodegeneration (Arcuri et al., 2017; Yanuck, 2019).

Motility studies showed that PCD-type cells in all microglia cultures are more mobile than WT-type cells. These findings suggest that mutations in the *Ccp1* gene may also influence microglial motility, in this case

by enhancing it. As previously discussed, the CCP1 protein is essential for the stabilisation of microtubules within the cytoskeleton (Muñoz-Castañeda et al., 2018). Microtubules are known to restrict cell movement and regulate directional migration (Ganguly et al., 2012). This could explain the increased and less directed motility observed in PCD microglial cultures, as cells do not have control over the microtubule dynamics of their cytoskeleton (Adrian et al., 2023; Rosito et al., 2023). As extensively documented, microglial cells actively scan the brain parenchyma by physically interacting with other cells, contributing to the structural shape of the brain and the stabilisation of neuronal connections (Nebeling et al., 2023). In the PCD mouse, altered microglial motility may compromise these essential functions (Franco-Bocanegra et al., 2019). Indeed, several studies have shown that altered or misdirected microglial motility can promote the development of a pro-inflammatory phenotype (Gyoneva et al., 2016; Franco-Bocanegra et al., 2019). In addition, as with phagocytosis, impaired motility may hinder microglia synaptic pruning, potentially leading to aberrant neuronal connectivity that could trigger the death of certain neurons (Arcuri et al., 2017). Ongoing studies in our laboratory indicate that the synapses established in the cerebellum of PCD mice are altered even before the onset of neurodegenerative processes. Moreover, previous research has shown that altered microglia motility can interfere with key functions such as phagocytosis and immune response (Franco-Bocanegra et al., 2019; Bernier et al., 2020). A similar phenomenon appears to occur in our PCD model of neurodegeneration, where altered microglial motility is accompanied by impaired phagocytic activity and immune responsiveness. These findings suggest that altered microglial motility in PCD mice could affect proper phagocytosis and immune response.

Finally, cell proliferation studies revealed that PCD BMDML cells exhibited a higher proliferative capacity compared to WT cells. Thus, mutations in the *Ccp1* gene appear to increase cell division. One possible explanation is the reduced differentiation status of BMDML cells, as they remain in a more undifferentiated state and probably have a greater proliferative capacity (Zhu & Skoultchi, 2001; Ye et al., 2018). However, when examining the proliferation capacity of microglial cells isolated from the cerebral cortex, no clear differences were observed between the two genotypes. Therefore, although *Ccp1* mutations promote microglia proliferation, a healthy neuronal environment can maintain this proliferation under homeostatic conditions, like those observed in WT models (Wang et al., 2011; Oria et al., 2018). Notably, in a degenerative neural environment, microglia proliferation was again elevated in PCD mice in response to the neurodegenerative processes occurring in both the cerebellum and OB, as observed in our *in vivo* studies (see below). Importantly, these *in vitro* findings complement previous *in vivo* observations from our laboratory, which demonstrated significantly increased microglial proliferation and turnover in PCD mice, as evidenced by elevated 5-bromo-2′-deoxyuridine (BrdU) incorporation in microglia from the cerebellum and OB (Baltanás et al., 2013). Together, these data support the notion that *Ccp1* inactivation is associated with an altered microglial proliferative phenotype both *in vitro* and *in vivo*. Future studies using microglia-specific conditional *Ccp1* knockout models will be essential to definitively determine the cell-autonomous contribution of CCP1 to microglial dysfunction and to disentangle intrinsic effects from those driven by the neurodegenerative environment. In addition, future studies employing cell type–specific overexpression of *Ccp1* may further complement loss-of-function approaches and help refine the understanding of CCP1 function across distinct neural and glial populations.

Following the completion of all *in vitro* analyses, we next examined the status of the microglia in PCD mice *in vivo*—before, during, and after the neurodegenerative processes occurring in both the cerebellum and OB.

Prior to the onset of neurodegenerative processes in both regions, an elevated expression of some general microglial markers of phagocytosis, motility, and inflammatory responses (both pro-inflammatory and anti-inflammatory) was observed. Notably, a similar pattern was identified in the gene expression analysis of PCD BMDML cells, which also showed increased expression of markers related to motility and pro-inflammatory activity. These findings suggest that microglial activation may occur even before the start of neurodegeneration (Vezzani et al., 2013; Fu et al., 2014; Zheng et al., 2016; Franco-Bocanegra et al., 2019). Such activation may be explained by two non-mutually exclusive hypotheses. First, mutations in the *Ccp1* gene may predispose microglia to impaired functioning, as previously discussed. Second, previous studies from our laboratory have shown that there are certain ultrastructural and morphological alterations in Purkinje (Baltanás et al., 2011; Muñoz-Castañeda et al., 2018; Pérez-Revuelta et al., 2025) and mitral cells (Valero et al., 2006) of PCD mice even before overt neurodegeneration becomes apparent. These findings indicate that microglia may be capable of detecting subtle cellular dysfunctions or environmental changes and responding accordingly, likely to maintain homeostasis within the neural system (Colonna & Butovsky, 2017).

During the peak of neurodegeneration in both the cerebellum and OB, an elevated expression of nearly all microglial markers analysed was observed. This result indicates that microglia are highly activated in both brain regions, most likely as a response to the degeneration of Purkinje and mitral cells (Landis & Mullen, 1978; Recio et al., 2007; Valero et al., 2007; Wang & Morgan, 2007;Muñoz-Castañeda et al., 2018). Moreover, immunohistochemical analysis using Iba1 revealed an increase in microglial density in both the cerebellum and OB of PCD mice, consistent with previous findings at comparable ages (Baltanás et al., 2013; Pérez-Martín et al., 2023). In parallel, the upregulation of genes associated with phagocytosis and motility further supports an enhancement of these microglial functions. As observed in various neurodegenerative pathologies, microglia in PCD mice appear to adopt an activated phenotype, characterised by increased motility and phagocytic capacity. This activation likely facilitates their migration through the neural parenchyma towards dead neurons, enabling their clearance from the surrounding environment to restore homeostasis (Neher et al., 2012; Butler et al., 2021; Gao et al., 2023). Moreover, in both the cerebellum and OB, microglia tend to migrate towards layers where degenerating neurons are located (Baltanás et al., 2013; Pérez-Martín et al., 2023), a phenomenon that is more evident in the cerebellum. This effect may be attributed to the more rapid and aggressive degeneration of Purkinje cells compared to mitral cells, potentially eliciting a stronger microglial response. These observations are consistent with the *in vitro* results, where PCD microglia isolated from the cerebellum and OB exhibited greater phagocytosis and motility than WT microglia. Furthermore, in both the cerebellum and OB of PCD mice, we observed increased expression of the Iba1 marker, probably because of the neurodegenerative processes occurring in these regions (Michalski et al., 2017; Ousta et al., 2022). This *in vivo* result is consistent with our *in vitro* findings, where microglia isolated from the cerebellum and OB of PCD mice exhibited elevated Iba1 expression. In contrast, cultures of BMDML or cortical cells showed reduced Iba1 expression in PCD mice. These results suggest that microglia from PCD mice only exhibit abnormally elevated levels of Iba1 when situated within a neurodegenerative environment.

Additionally, while the microglial morphology during the pre-neurodegenerative phase was predominantly branched, the morphology observed during peak neurodegeneration was primarily amoeboid and/or hyper-ramified—both of which are associated with microglial activation states (Parakalan et al., 2012; Boche et al., 2013; Vidal-Itriago et al., 2022; Adrian et al., 2023). This morphological change in response to neuronal damage was also observed in our *in vitro* experiments. Specifically, we observed an increase in cell area and a reduction in tracking area, consistent with the morphological changes observed in cultured microglia isolated from the cerebellum and OB at the same age. Notably, previous studies have shown that an increase in microglial cell area is indicative of activation in response to noxious stimuli (Davis et al., 2017).

Likewise, the increased expression of immune response genes likely

corresponds to an elevated release of both pro-inflammatory and anti-inflammatory mediators. In the PCD model, this release appears to be massive and uncontrolled, potentially exacerbating neuronal death in both Purkinje and mitral cells and contributing to additional damage in the surrounding neural tissue (Zheng et al., 2016). This hypothesis aligns with our observations in the cerebellum, where the release of inflammatory mediators is particularly intense and significantly higher than in the OB. This may help explain the rapid and abrupt degeneration of Purkinje cell death. In contrast, although the OB also shows elevated expression of inflammatory response genes, the levels are comparatively lower than what is observed in the cerebellum, which could account for the slower and more gradual degeneration of mitral cells over time. Importantly, regional differences in the speed, intensity, and nature of neuronal degeneration may contribute to explaining the apparent predominance of anti-inflammatory markers in degenerative regions (Colonna & Butovsky, 2017; Neher & Cunningham, 2019). In the cerebellum, the rapid and markedly inflammatory degeneration of Purkinje cells likely induces an intense and acute microglial activation, which may rapidly shift towards an anti-inflammatory or resolution phenotype as a mechanism to limit collateral damage in the surrounding tissue. In contrast, the slower and more progressive loss of mitral cells in the OB may favour a more sustained microglial activation state, with a relatively greater contribution of anti-inflammatory signals. Taken together, these findings suggest that the combination of *Ccp1* loss-of-function and the region-specific neurodegenerative context leads to distinct microglial activation profiles, rather than to a uniform inflammatory response. In this context, it is important to note that the intensity of CD45 immunoreactivity may differ markedly between brain regions. Microglia in the OB have been reported to display lower basal levels of CD45 expression and a less immunologically primed phenotype compared with microglia in other regions, including the cerebellum. This well-established regional heterogeneity likely contributes to the weaker CD45 signal observed in the OB, despite increased microglial density or activation during neurodegeneration (de Haas et al., 2008; Grabert et al., 2016). However, it is also important to consider that the OB is a highly plastic region, capable of adapting to various abnormal or pathological conditions (Díaz et al., 2017; Pérez-Boyero et al., 2023). This plasticity may confer greater resistance to neurodegenerative processes, making them less severe or pronounced (Díaz et al., 2017). Additionally, microtubule dysfunction in certain types of glial cells has been linked to the development of neurodegenerative processes, likely due to dysregulation of their immune responses (Cyske et al., 2023). Thus, mutations in the *Ccp1* gene may predispose PCD microglia to excessive and uncontrolled immune activation, possibly because of abnormal microtubule function.

Following the completion of primary neurodegenerative processes, both the cerebellum and OB maintained microglial density, distribution, and morphology like those found during their respective peaks of neuronal death. Both regions also presented elevated levels of markers associated with phagocytic capacity, motility, and immune response, although these levels were lower than those produced during active neurodegeneration. Interestingly, this sustained expression was more pronounced in the OB, where an upregulation of nearly all genes analysed persisted into the post-degenerative period, albeit at levels lower than that observed during the neuronal degeneration phase itself. These findings suggest the presence of a chronic microglial response, which may contribute to the continued death of both mitral cells and other neuronal populations. Indeed, previous studies on the OB of PCD mice have reported not only mitral cell loss but also the death of certain interneurons (Valero et al., 2007). This secondary degeneration could be driven by sustained microglial activation (Recio et al., 2007; Valero et al., 2007). Furthermore, the persistent state of increased activation observed in the OB may reflect the fact that bulbar degeneration is not yet fully completed. Traditionally, it is considered that by P110, virtually all mitral cells have degenerated in PCD mice (Valero et al., 2007). However, there is no clear consensus regarding the exact timing of this degeneration, with some studies suggesting it concludes around P90, while others report it may extend to P120 or beyond (Greer & Shepherd, 1982; Recio et al., 2011; Díaz et al., 2012). A similar phenomenon is observed in lobe X of the cerebellum, which exhibits a particular resistance to Purkinje cell degeneration, with the loss of these neurons occurring at a later stage (Hernández-Pérez et al., 2023; Hernández-Pérez et al., 2025).

5. Conclusions

In summary, our findings highlight the remarkable versatility of microglia and underscore the importance of integrating both *in vitro* and *in vivo* models when studying their behaviour. As demonstrated in this study, even subtle variations in the cellular environment can significantly influence microglial characteristics and functions. We show that microglia in PCD mice exhibit abnormal behaviour due to the mutation in the *Ccp1* gene, which disrupts fundamental microglial functions such as phagocytosis, motility, and immune response. These impairments affect the way microglia respond to stimuli, leading to their poorly regulated and exacerbated reactions that contribute to the establishment of a neurodegenerative environment and promote neuronal loss along with a loss of motor skills. The consequences of microglia dysfunction in PCD mice are further supported by previous research from our laboratory. We have shown that transplanted healthy bone marrow cells differentiate into microglia within nervous tissue, resulting in reduced neuronal death in PCD mice. This neuroprotection is likely due to the proper functioning of healthy microglia, which may counteract the altered effects of mutant microglia (Díaz et al., 2012). These findings suggest that future research should explore the complete replacement of impaired microglia in PCD mice with healthy microglia to assess the impact on neurodegeneration in both the cerebellum and OB. Similar mechanisms have been observed in other neurodegenerative diseases, where microglia malfunction can trigger or exacerbate neuronal loss. For all these reasons, investigating how microglia respond to different neurodegenerative diseases is critical. A deeper understanding of microglia function could pave the way for novel therapeutic strategies for treating neurodegenerative diseases, as well as new diagnostic tools. In this study, we observed that microglia in both the cerebellum and OB of PCD mice exhibit an activated profile, characterised by the release of specific inflammatory cytokines even before the onset of neurodegenerative processes. These molecules may serve as early biomarkers for certain neurological pathologies, potentially enabling early diagnosis and treatment (Benatar et al., 2022; Wilson et al., 2023; Mészáros & Guizzaro, 2024).

In conclusion, this work highlights the pivotal role of microglia in the development of neurodegenerative diseases. Fully understanding the functional dynamics of these cells is essential, as even minor disruptions in their core activities can trigger major neurodegenerative processes.

CRediT authorship contribution statement

David Pérez-Boyero: Writing – review & editing, Writing – original draft, Visualization, Validation, Software, Resources, Project administration, Methodology, Investigation, Funding acquisition, Formal analysis, Data curation, Conceptualization. **Ana de la Mata:** Methodology, Investigation, Formal analysis. **Jesus Castillo-Sanchez:** Investigation, Formal analysis. **Ingrid Reverte:** Methodology, Investigation, Formal analysis. **Natalia Yanguas-Casás:** Methodology, Investigation, Formal analysis. **Carmelo Ávila-Zarza:** Formal analysis, Data curation. **Jorge Valero:** Methodology, Formal analysis, Data curation. **José R. Alonso:** Resources, Funding acquisition. **Maria-Angeles Arevalo:** Resources, Methodology, Investigation, Formal analysis, Data curation. **Davide Ragozzino:** Resources, Methodology, Investigation. **Eduardo Weruaga:** Writing – review & editing, Visualization, Validation, Supervision, Software, Resources, Project administration, Methodology, Investigation, Funding acquisition, Formal analysis, Data curation,

Conceptualization. **David Díaz:** Writing – review & editing, Visualization, Validation, Supervision, Software, Resources, Project administration, Methodology, Investigation, Funding acquisition, Formal analysis, Data curation, Conceptualization.

Declaration of competing interest

The authors declare that they have no known competing financial interests or personal relationships that could have appeared to influence the work reported in this paper.

Acknowledgments

We express our gratitude to María Sánchez, Dr. Rocio Talaverón, Elisa Baides, Dr. Daniel Pinto, Dr. Giorgia Scaringi, Dr. Laura Ferrucci for technical support, and Emma Keck for revising the English.

Funding.

This research was funded by the Spanish Ministry of Economy and Competitiveness (MINECO; SAF2016-79668-R), the Spanish Ministry of Science Innovation (MICINN; PID2019-106943RB-I00 and PID2022-140456NB-I00; Research Network RED2022-134081-T), and the Regional Government of Castile and Leon (SA129P20 and SA112P24). Work by D.P.-B. was supported by a predoctoral contract from the University of Salamanca, co-funded by Banco Santander. Additional support was provided by an EMBO Scientific Exchange Grant (grant no. 9825), which supports international collaborations.

Ethics Declarations.

Ethics approval and consent to participate.

Animal experiments were conducted in compliance with the guidelines established by European (Directive 2010/63/EU, Recommendation 2007/526/EC) and Spanish (Law 32/2007, Royal Decree 53/2013) legislation. All the experiments were approved by the Bioethics Committee of the University of Salamanca (reference number: #00613). All authors consent to participate in this manuscript.

Appendix A. Supplementary data

Supplementary data to this article can be found online at https://doi.org/10.1016/j.bbi.2025.106248.

Data availability

Data will be made available on request.

References

Adrian, M., Weber, M., Tsai, M.C., Glock, C., Kahn, O.I., Phu, L., et al., 2023. Polarized microtubule remodeling transforms the morphology of reactive microglia and drives cytokine release. Nat. Commun. 14, 6322. https://doi.org/10.1038/s41467-023-41891-6.

Arcuri, C., Mecca, C., Bianchi, R., Giambanco, I., Donato, R., 2017. The pathophysiological role of microglia in dynamic surveillance, phagocytosis and structural remodeling of the developing CNS. Front. Mol. Neurosci. 10, 191. https://doi.org/10.3389/fnmol.2017.00191.

Baltanás, F.C., Berciano, M.T., Santos, E., Lafarga, M., 2021. The childhood-onset neurodegeneration with cerebellar atrophy (CONDCA) disease caused by AGTPBP1 gene mutations: the Purkinje cell degeneration mouse as an animal model for the study of this human disease. Biomedicines 9, 1157. https://doi.org/10.3390/biomedicines9091157.

Baltanás, F.C., Berciano, M.T., Valero, J., Gómez, C., Díaz, D., Alonso, J.R., et al., 2013. Differential glial activation during the degeneration of Purkinje cells and mitral cells in the PCD mutant mice. Glia 61, 254–272. https://doi.org/10.1002/glia.22431.

Baltanás, F.C., Casafont, I., Weruaga, E., Alonso, J.R., Berciano, M.T., Lafarga, M., et al., 2011. Nucleolar disruption and Cajal body disassembly are nuclear hallmarks of DNA damage-induced neurodegeneration in Purkinje cells. Brain Pathol. 21, 374–388. https://doi.org/10.1111/j.1750-3639.2010.00461.x.

Basilico, B., Ferrucci, L., Ratano, P., Golia, M.T., Grimaldi, A., Rosito, M., et al., 2022. Microglia control glutamatergic synapses in the adult mouse hippocampus. Glia 70, 173–195. https://doi.org/10.1002/glia.24101.

Beccari, S., Sierra-Torre, V., Valero, J., Pereira-Iglesias, M., García-Zaballa, M., Soria, F. N., et al., 2023. Microglial phagocytosis dysfunction in stroke is driven by energy depletion and induction of autophagy. Autophagy 19, 1952–1981. https://doi.org/10.1080/15548627.2023.2165313.

Benatar, M., Wuu, J., McHutchison, C., Postuma, R.B., Boeve, B.F., Petersen, R., et al., 2022. First International Pre-Symptomatic ALS Workshop: preventing amyotrophic lateral sclerosis—insights from pre-symptomatic neurodegenerative diseases. Brain 145, 27–44. https://doi.org/10.1093/brain/awab404.

Berezniuk, I., Vu, H.T., Lyons, P.J., Sironi, J.J., Xiao, H., Burd, B., et al., 2012. Cytosolic carboxypeptidase 1 is involved in processing α- and β-tubulin. J. Biol. Chem. 287, 6503–6517. https://doi.org/10.1074/jbc.M111.309138.

Bernier, L.P., York, E.M., Kamyabi, A., Choi, H.B., Weilinger, N.L., MacVicar, B.A., 2020. Microglial metabolic flexibility supports immune surveillance of the brain parenchyma. Nat. Commun. 11, 1559. https://doi.org/10.1038/s41467-020-15267-z.

Bhusal, A., Ortega, A., Suk, K., 2023. Editorial: dysfunctional microglia in neurological disorders. Front. Cell. Neurosci. 17, 1133019. https://doi.org/10.3389/fncel.2023.1133019.

Boche, D., Perry, V.H., Nicoll, J.A.R., 2013. Review: activation patterns of microglia and their identification in the human brain. Neuropathol. Appl. Neurobiol. 39, 3–18. https://doi.org/10.1111/nan.12011.

Bronstein, R., Torres, L., Nissen, J.C., Tsirka, S.E., 2013. Culturing microglia from the neonatal and adult central nervous system. J. Vis. Exp. 78, e50647. https://doi.org/10.3791/50647.

Butler, C.A., Popescu, A.S., Kitchener, E.J.A., Allendorf, D.H., Puigdellívol, M., Brown, G. C., 2021. Microglial phagocytosis of neurons in neurodegeneration, and its regulation. J. Neurochem. 158, 621–639. https://doi.org/10.1111/jnc.15327.

Chen, W., Zhang, Y., Zhai, X., Xie, L., Guo, Y., Chen, C., et al., 2022. Microglial phagocytosis and regulatory mechanisms after stroke. J. Cereb. Blood Flow Metab. 42, 1579–1596. https://doi.org/10.1177/0271678X221098841.

Cheng, J., Liao, Y., Dong, Y., Hu, H., Yang, N., Kong, X., et al., 2020. Microglial autophagy defect causes Parkinson disease-like symptoms by accelerating inflammasome activation in mice. Autophagy 16, 2193–2205. https://doi.org/10.1080/15548627.2020.1719723.

Colonna, M., Butovsky, O., 2017. Microglia function in the central nervous system during health and neurodegeneration. Annu. Rev. Immunol. 35, 441–468. https://doi.org/10.1146/annurev-immunol-051116-052358.

Cyske, Z., Gaffke, L., Pierzynowska, K., Węgrzyn, G., 2023. Tubulin cytoskeleton in neurodegenerative diseases—not only primary tubulinopathies. Cell. Mol. Neurobiol. 43, 1867–1884. https://doi.org/10.1007/s10571-022-01304-6.

Czekanska, E.M., 2011. Assessment of cell proliferation with resazurin-based fluorescent dye. Methods Mol. Biol. 740, 27–32. https://doi.org/10.1007/978-1-61779-108-6_5.

Daniele, S.G., Edwards, A.A., Maguire-Zeiss, K.A., 2014. Isolation of cortical microglia with preserved immunophenotype and functionality from murine neonates. J. Vis. Exp. 83, e51005. https://doi.org/10.3791/51005.

Davis, B.M., Salinas-Navarro, M., Cordeiro, M.F., Moons, L., De Groef, L., 2017. Characterizing microglia activation: a spatial statistics approach to maximize information extraction. Sci. Rep. 7, 1576. https://doi.org/10.1038/s41598-017-01747-8.

de Haas, A.H., Boddeke, H.W., Biber, K., 2008. Region-specific expression of immunoregulatory proteins on microglia in the healthy CNS. Glia 56, 888–894. https://doi.org/10.1002/glia.20663.

Del Pilar, C., Garrido-Matilla, L., Del Pozo-Filíu, L., Lebrón-Galán, R., Arias, R.F., Clemente, D., et al., 2024. Intracerebellar injection of monocytic immature myeloid cells prevents the adverse effects caused by stereotactic surgery in a model of cerebellar neurodegeneration. J. Neuroinflammation 21, 49. https://doi.org/10.1186/s12974-023-03000-8.

Del Pilar, C., Lebrón-Galán, R., Pérez-Martín, E., Pérez-Revuelta, L., Ávila-Zarza, C.A., Alonso, J.R., et al., 2021. The selective loss of Purkinje cells induces specific peripheral immune alterations. Front. Cell. Neurosci. 15, 773696. https://doi.org/10.3389/fncel.2021.773696.

Díaz, D., Muñoz-Castañeda, R., Ávila-Zarza, C., Carretero, J., Alonso, J.R., et al., 2017. Olfactory bulb plasticity ensures proper olfaction after severe impairment in postnatal neurogenesis. Sci. Rep. 7, 5654. https://doi.org/10.1038/s41598-017-05970-1.

Díaz, D., Recio, J.S., Weruaga, E., Alonso, J.R., 2012. Mild cerebellar neurodegeneration of aged heterozygous PCD mice increases cell fusion of Purkinje and bone marrow-derived cells. Cell Transplant. 21, 1595–1602. https://doi.org/10.3727/096368912X638900.

Doorn, K.J., Brevé, J.J., Drukarch, B., Boddeke, H.W., Huitinga, I., Lucassen, P.J., et al., 2015. Brain region-specific gene expression profiles in freshly isolated rat microglia. Front. Cell. Neurosci. 9, 84. https://doi.org/10.3389/fncel.2015.00084.

Fernandez-Gonzalez, A., La Spada, A.R., Treadaway, J., Higdon, J.C., Harris, B.S., Sidman, R.L., et al., 2002. Purkinje cell degeneration (pcd) phenotypes caused by mutations in the axotomy-induced gene, Nna1. Science 295, 1904–1906. https://doi.org/10.1126/science.1068912.

Franco-Bocanegra, D.K., McAuley, C., Nicoll, J.A.R., Boche, D., 2019. Molecular mechanisms of microglial motility: changes in ageing and Alzheimer's disease. Cells 8, 639. https://doi.org/10.3390/cells8060639.

Fu, R., Shen, Q., Xu, P., Luo, J.J., Tang, Y., 2014. Phagocytosis of microglia in the central nervous system diseases. Mol. Neurobiol. 49, 1422–1434. https://doi.org/10.1007/s12035-013-8620-6.

Ganguly, A., Yang, H., Sharma, R., Patel, K.D., Cabral, F., 2012. The role of microtubules and their dynamics in cell migration. J. Biol. Chem. 287, 43359–43369. https://doi.org/10.1074/jbc.M112.423905.

Gao, C., Jiang, J., Tan, Y., Chen, S., 2023. Microglia in neurodegenerative diseases: mechanism and potential therapeutic targets. Signal Transduct. Target. Ther. 8, 359. https://doi.org/10.1038/s41392-023-01588-0.

Goldmann, T., Prinz, M., 2013. Role of microglia in CNS autoimmunity. Clin. Dev. Immunol. 2013, 208093. https://doi.org/10.1155/2013/208093.
Grabert, K., Michoel, T., Karavolos, M.H., Clohisey, S., Baillie, J.K., Stevens, M.P., et al., 2016. Microglial brain region-dependent diversity and selective regional sensitivities to aging. Nat. Neurosci. 19, 504–516. https://doi.org/10.1038/nn.4222.
Greer, C.A., Shepherd, G.M., 1982. Mitral cell degeneration and sensory function in the neurological mutant mouse Purkinje cell degeneration (PCD). Brain Res. 235, 156–161. https://doi.org/10.1016/0006-8993(82)90206-2.
Guo, Y., Hong, W., Wang, X., Zhang, P., Körner, H., Tu, J., et al., 2019. MicroRNAs in microglia: how do microRNAs affect activation, inflammation, polarization of microglia and mediate the interaction between microglia and glioma? Front. Mol. Neurosci. 12, 125. https://doi.org/10.3389/fnmol.2019.00125.
Gyoneva, S., Swanger, S.A., Zhang, J., Weinshenker, D., Traynelis, S.F., 2016. Altered motility of plaque-associated microglia in a model of Alzheimer's disease. Neuroscience 330, 410–420. https://doi.org/10.1016/j.neuroscience.2016.05.061.
Hashimoto, K., Kano, M., 2013. Synapse elimination in the developing cerebellum. Cell. Mol. Life Sci. 70, 4667–4680. https://doi.org/10.1007/s00018-013-1405-2.
Henry, R.J., Ritzel, R.M., Barrett, J.P., Doran, S.J., Jiao, Y., Leach, J.B., et al., 2020. Microglial depletion with CSF1R inhibitor during chronic phase of experimental traumatic brain injury reduces neurodegeneration and neurological deficits. J. Neurosci. 40, 2960–2974. https://doi.org/10.1523/JNEUROSCI.2402-19.2020.
Hernández-Pérez, C., Calderón-García, A.A., Pérez-Boyero, D., González-Núñez, V., Weruaga, E., Díaz, D., 2025. Specific glutamylation patterns of the cytoskeleton confer neuroresistance to lobe X of the cerebellum in a model of childhood-onset neurodegeneration with cerebellar atrophy. Int. J. Mol. Sci. 26, 10378. https://doi.org/10.3390/ijms262110378.
Hernández-Pérez, C., Weruaga, E., Díaz, D., 2023. Lobe X of the cerebellum: a natural neuro-resistant region. Anatomia 2, 43–62. https://doi.org/10.3390/anatomia2010005.
Herzog, C., Pons Garcia, L., Keatinge, M., Greenald, D., Moritz, C., Peri, F., et al., 2019. Rapid clearance of cellular debris by microglia limits secondary neuronal cell death after brain injury in vivo. Development 146, dev174698. https://doi.org/10.1242/dev.174698.
Hinze, A., Stolzing, A., 2011. Differentiation of mouse bone marrow-derived stem cells toward microglia-like cells. BMC Cell Biol. 12, 35. https://doi.org/10.1186/1471-2121-12-35.
Hinze, A., Stolzing, A., 2012. Microglia differentiation using a culture system for the expansion of mice non-adherent bone marrow stem cells. J. Inflamm. 9, 12. https://doi.org/10.1186/1476-9255-9-12.
Human Protein Atlas. (2025) AGTPBP1 expression in cell types. The Human Protein Atlas. Available at: https://www.proteinatlas.org/ENSG00000135049-AGTPBP1/tissue (accessed 1 December 2025).
Illes, P., Rubini, P., Ulrich, H., Zhao, Y., Tang, Y., 2020. Regulation of microglial functions by purinergic mechanisms in the healthy and diseased CNS. Cells 9, 1108. https://doi.org/10.3390/cells9051108.
Kaiser, T., Feng, G., 2019. Tmem119-EGFP and Tmem119-CreERT2 transgenic mice for labeling and manipulating microglia. eNeuro 6, ENEURO.0448-18.2019. https://doi.org/10.1523/ENEURO.0448-18.2019.
Karakaya, M., Paketci, C., Altmueller, J., Thiele, H., Hoelker, I., Yis, U., et al., 2019. Biallelic variant in AGTPBP1 causes infantile lower motor neuron degeneration and cerebellar atrophy. Am. J. Med. Genet. A 179, 1580–1584. https://doi.org/10.1002/ajmg.a.61198.
Kodali, M., Madhu, L.N., Somayaji, Y., Attaluri, S., Huard, C., Panda, P.K., et al., 2025. Residual microglia following short-term PLX5622 treatment in 5xFAD mice exhibit diminished NLRP3 inflammasome and mTOR signaling, and enhanced autophagy. Aging Cell 24, e14398. https://doi.org/10.1111/acel.14398.
Kumar P, Nagarajan A, Uchil PD. (2018) Analysis of cell viability by the alamarBlue assay. Cold Spring Harb. Protoc. 2018, pdb.prot095489. https://doi.org/10.1101/pdb.prot095489.
Landis, S.C., Mullen, R.J., 1978. The development and degeneration of Purkinje cells in pcd mutant mice. J Comp Neurol 177, 125–143. https://doi.org/10.1002/cne.901770109.
Lee, J.K., Tansey, M.G., 2013. Microglia isolation from adult mouse brain. Methods Mol. Biol. 1041, 17–23. https://doi.org/10.1007/978-1-62703-520-0_3.
Li, Y., Tan, M.S., Jiang, T., Tan, L., 2014. Microglia in Alzheimer's disease. Biomed Res. Int. 2014, 437483. https://doi.org/10.1155/2014/437483.
Lin, D.M., Wang, F., Lowe, G., Gold, G.H., Axel, R., Ngai, J., et al., 2000. Formation of precise connections in the olfactory bulb occurs in the absence of odorant-evoked neuronal activity. Neuron 26, 69–80. https://doi.org/10.1016/s0896-6273(00)81139-3.
Mészáros, L., Guizzaro, L., 2024. Developing medicines for the pre-symptomatic stage of degenerative neurological conditions: challenges and opportunities. Rev. Neurol. (Paris) 180, 141–146. https://doi.org/10.1016/j.neurol.2023.06.002.
Mhatre, S.D., Tsai, C.A., Rubin, A.J., James, M.L., Andreasson, K.I., 2015. Microglial malfunction: the third rail in the development of Alzheimer's disease. Trends Neurosci. 38, 621–636. https://doi.org/10.1016/j.tins.2015.08.006.
Michalski, D., Pitsch, R., Pillai, D.R., Mages, B., Aleithe, S., Grosche, J., et al., 2017. Delayed histochemical alterations within the neurovascular unit due to transient focal cerebral ischemia and experimental treatment with neurotrophic factors. PLoS One 12, e0174996. https://doi.org/10.1371/journal.pone.0174996.
Möller, K., Brambach, M., Villani, A., Gallo, E., Gilmour, D., et al., 2022. A Role for the Centrosome in Regulating the Rate of Neuronal Efferocytosis by Microglia in Vivo. elife 11, e82094. https://doi.org/10.7554/eLife.82094.
Muñoz-Castañeda, R., Díaz, D., Peris, L., Andrieux, A., Bosc, C., Muñoz-Castañeda, J.M., et al., 2018. Cytoskeleton stability is essential for the integrity of the cerebellum and its motor- and affective-related behaviors. Sci. Rep. 8, 3072. https://doi.org/10.1038/s41598-018-21470-2.
Nebeling, F.C., Poll, S., Justus, L.C., Steffen, J., Keppler, K., Mittag, M., et al., 2023. Microglial Motility Is Modulated by Neuronal Activity and Correlates with Dendritic Spine Plasticity in the Hippocampus of Awake Mice. elife 12, e83176. https://doi.org/10.7554/eLife.83176.
Neher, J.J., Cunningham, C., 2019. Priming microglia for innate immune memory in the brain. Trends Immunol. 40, 358–374. https://doi.org/10.1016/j.it.2019.02.001.
Neher, J.J., Neniskyte, U., Brown, G.C., 2012. Primary phagocytosis of neurons by inflamed microglia: potential roles in neurodegeneration. Front. Pharmacol. 3, 27. https://doi.org/10.3389/fphar.2012.00027.
Oria, M., Figueira, R.L., Scorletti, F., Sbragia, L., Owens, K., Li, Z., et al., 2018. CD200–CD200R imbalance correlates with microglia and pro-inflammatory activation in rat spinal cords exposed to amniotic fluid in retinoic acid-induced spina bifida. Sci. Rep. 8, 10638. https://doi.org/10.1038/s41598-018-28829-5.
Ousta, A., Piao, L., Fang, Y.H., Vera, A., Nallamothu, T., Garcia 3rd, A.J., et al., 2022. Microglial activation and neurological outcomes in a murine model of cardiac arrest. Neurocrit. Care 36, 61–70. https://doi.org/10.1007/s12028-021-01253-w.
Paasila, P.J., Davies, D.S., Kril, J.J., Goldsbury, C., Sutherland, G.T., 2019. The relationship between the morphological subtypes of microglia and Alzheimer's disease neuropathology. Brain Pathol. 29, 726–740. https://doi.org/10.1111/bpa.12717.
Parakalan, R., Jiang, B., Nimmi, B., Janani, M., Jayapal, M., Lu, J., et al., 2012. Transcriptome analysis of amoeboid and ramified microglia isolated from the corpus callosum of rat brain. BMC Neurosci. 14, 64. https://doi.org/10.1186/1471-2202-13-64.
Pasko, V.I., Churkina, A.S., Shakhov, A.S., Kotlobay, A.A., Alieva, I.B., 2023. Modeling of neurodegenerative diseases: "step by step" and "network" organization of the complexes of model systems. Int. J. Mol. Sci. 24, 604. https://doi.org/10.3390/ijms24010604.
Pérez-Boyero, D., Hernández-Pérez, C., Valero, J., Cabedo, V.L., Alonso, J.R., Díaz, D., et al., 2023. The eNOS isoform exhibits increased expression and activation in the main olfactory bulb of nNOS knock-out mice. Front. Cell. Neurosci. 17, 1120836. https://doi.org/10.3389/fncel.2023.1120836.
Pérez-Martín, E., Pérez-Revuelta, L., Barahona-López, C., Pérez-Boyero, D., Alonso, J.R., Díaz, D., et al., 2023. Oleoylethanolamide treatment modulates both neuroinflammation and microgliosis, and prevents massive leukocyte infiltration to the cerebellum in a mouse model of neuronal degeneration. Int. J. Mol. Sci. 24, 9691. https://doi.org/10.3390/ijms24119691.
Pérez-Revuelta, L., Pérez-Boyero, D., Pérez-Martín, E., Cabedo, V.L., Téllez de Meneses, P.G., Weruaga, E., et al., 2025. Neuroprotective effects of VEGF-B in a murine model of aggressive neuronal loss with childhood onset. Int. J. Mol. Sci. 26, 538. https://doi.org/10.3390/ijms26020538.
Podleśny-Drabiniok, A., Marcora, E., Goate, A.M., 2020. Microglial phagocytosis: a disease-associated process emerging from Alzheimer's disease genetics. Trends Neurosci. 43, 965–979. https://doi.org/10.1016/j.tins.2020.10.002.
Ramadan, Y.H., Gu, A., Ross, N., McEwan, S.A., Barr, M.M., Firestein, B.L., et al., 2021. CCP1, a Tubulin Deglutamylase, Increases Survival of Rodent Spinal Cord Neurons following Glutamate-Induced Excitotoxicity. eNeuro 8, 0431. https://doi.org/10.1523/ENEURO.0431-20.2021.
Recio, J.S., Álvarez-Dolado, M., Díaz, D., Baltanás, F.C., Piquer-Gil, M., Alonso, J.R., et al., 2011. Bone marrow contributes simultaneously to different neural types in the central nervous system through different mechanisms of plasticity. Cell Transplant. 20, 1179–1192. https://doi.org/10.3727/096368910X552826.
Recio, J.S., Weruaga, E., Gómez, C., Valero, J., Briñón, J.G., Alonso, J.R., 2007. Changes in the connections of the main olfactory bulb after mitral cell selective neurodegeneration. J. Neurosci. Res. 85, 2407–2421. https://doi.org/10.1002/jnr.21387.
Riquier, A.J., Sollars, S.I., 2020. Astrocytic response to neural injury is larger during development than in adulthood and is not predicated upon the presence of microglia. Brain Behav. Immun. Health 1, 100010. https://doi.org/10.1016/j.bbih.2019.100010.
Rosito, M., Sanchini, C., Gosti, G., Moreno, M., De Panfilis, S., Giubettini, M., et al., 2023. Microglia reactivity entails microtubule remodeling from acentrosomal to centrosomal arrays. Cell Rep. 42, 112104. https://doi.org/10.1016/j.celrep.2023.112104.
Rossi, C., Cusimano, M., Zambito, M., Finardi, A., Capotondo, A., Garcia-Manteiga, J.M., et al., 2018. Interleukin 4 modulates microglia homeostasis and attenuates the early slowly progressive phase of amyotrophic lateral sclerosis. Cell Death Dis. 9, 250. https://doi.org/10.1038/s41419-018-0288-4.
Russell, W.M.S., Burch, R.L., 1959. The principles of humane experimental technique. Methuen and Co, London.
Salter, M.W., Stevens, B., 2017. Microglia emerge as central players in brain disease. Nat. Med. 23, 1018–1027. https://doi.org/10.1038/nm.4397.
Servet-Delprat, C., Arnaud, S., Jurdic, P., Nataf, S., Grasset, M.-F., Soulas, C., et al., 2002. Flt3+ macrophage precursors commit sequentially to osteoclasts, dendritic cells and microglia. BMC Immunol. 3, 15. https://doi.org/10.1186/1471-2172-3-15.
Shashi, V., Magiera, M.M., Klein, D., Zaki, M., Schoch, K., Rudnik-Schöneborn, S., et al., 2018. Loss of tubulin deglutamylase CCP1 causes infantile-onset neurodegeneration. EMBO J. 37, e100540. https://doi.org/10.15252/embj.2018100540.
Sillitoe, R.V., Joyner, A.L., 2007. Morphology, molecular codes, and circuitry produce the three-dimensional complexity of the cerebellum. Annu. Rev. Cell Dev. Biol. 23, 549–577. https://doi.org/10.1146/annurev.cellbio.23.090506.123237.
Spangenberg, E., Severson, P.L., Hohsfield, L.A., Crapser, J., Zhang, J., Burton, E.A., et al., 2019. Sustained microglial depletion with CSF1R inhibitor impairs

parenchymal plaque development in an Alzheimer's disease model. Nat. Commun. 10, 3758. https://doi.org/10.1038/s41467-019-11674-z.
Stojiljkovic, M.R., Schmeer, C., Witte, O.W., 2022. Pharmacological depletion of microglia leads to a dose-dependent reduction in inflammation and senescence in the aged murine brain. Neuroscience 488, 1–9. https://doi.org/10.1016/j.neuroscience.2022.02.018.
Sumpter, T.L., Packiam, V., Turnquist, H.R., Castellaneta, A., Yoshida, O., Thomson, A. W., 2011. DAP12 promotes IRAK-M expression and IL-10 production by liver myeloid dendritic cells and restrains their T cell allostimulatory ability. J. Immunol. 186, 1970–1980. https://doi.org/10.4049/jimmunol.1000527.
Valero, J., Berciano, M.T., Weruaga, E., Lafarga, M., Alonso, J.R., 2006. Pre-neurodegeneration of mitral cells in the PCD mutant mouse is associated with DNA damage, transcriptional repression, and reorganization of nuclear speckles and Cajal bodies. Mol. Cell. Neurosci. 33, 283–295. https://doi.org/10.1016/j.mcn.2006.08.002.
Valero, J., Weruaga, E., Murias, A.R., Recio, J.S., Curto, G.G., Gómez, C., et al., 2007. Changes in cell migration and survival in the olfactory bulb of the pcd/pcd mouse. Dev. Neurobiol. 67, 839–859. https://doi.org/10.1002/dneu.20352.
Vezzani, A., Aronica, E., Mazarati, A., Pittman, Q.J., 2013. Epilepsy and brain inflammation. Exp. Neurol. 244, 11–21. https://doi.org/10.1016/j.expneurol.2011.09.033.
Vidal-Itriago, A., Radford, R.A.W., Aramideh, J.A., Maurel, C., Scherer, N.M., Don, E.K., et al., 2022. Microglia morphophysiological diversity and its implications for the CNS. Front. Immunol. 13, 997786. https://doi.org/10.3389/fimmu.2022.997786.
Wang, K., Li, J., Zhang, Y., Huang, Y., Chen, D., Shi, Z., et al., 2021. Central nervous system diseases related to pathological microglial phagocytosis. CNS Neurosci. Ther. 27, 528–539. https://doi.org/10.1111/cns.13619.
Wang, T., Morgan, J.I., 2007. The Purkinje cell degeneration (pcd) mouse: an unexpected molecular link between neuronal degeneration and regeneration. Brain Res. 1140, 26–40. https://doi.org/10.1016/j.brainres.2006.07.065.
Wang, X.J., Zhang, S., Yan, Z.Q., Zhao, Y.X., Zhou, H.Y., Wang, Y., et al., 2011. Impaired CD200–CD200R-mediated microglia silencing enhances midbrain dopaminergic neurodegeneration: roles of aging, superoxide, NADPH oxidase, and p38 MAPK. Free Radic. Biol. Med. 50, 1094–1106. https://doi.org/10.1016/j.freeradbiomed.2011.01.032.
Wes, P.D., Sayed, F.A., Bard, F., Gan, L., 2016. Targeting microglia for the treatment of Alzheimer's disease. Glia 64, 1710–1732. https://doi.org/10.1002/glia.22988.
Wilson 3rd, D.M., Cookson, M.R., Van Den Bosch, L., Zetterberg, H., Holtzman, D.M., Dewachter, I., 2023. Hallmarks of neurodegenerative diseases. Cell 186, 693–714. https://doi.org/10.1016/j.cell.2022.12.032.
Wu, L., Kong, L., Yang, Y., Bian, X., Wu, S., Li, B., et al., 2019. Effects of cell differentiation on the phagocytic activities of IgM+ B cells in a teleost fish. Front. Immunol. 10, 2225. https://doi.org/10.3389/fimmu.2019.02225.
Wu, Q., Zou, C., 2022. Microglial dysfunction in neurodegenerative diseases via RIPK1 and ROS. Antioxidants 11, 2201. https://doi.org/10.3390/antiox11112201.
Yanguas-Casás, N., Crespo-Castrillo, A., Arevalo, M.A., Garcia-Segura, L.M., 2020. Aging and sex: impact on microglia phagocytosis. Aging Cell 19, e13182. https://doi.org/10.1111/acel.13182.
Yanuck, S.F., 2019. Microglial phagocytosis of neurons: diminishing neuronal loss in traumatic, infectious, inflammatory, and autoimmune CNS disorders. Front. Psych. 10, 712. https://doi.org/10.3389/fpsyt.2019.00712.
Ye, B., Liu, B., Hao, L., Zhu, X., Yang, L., Wang, S., et al., 2018. Klf4 glutamylation is required for cell reprogramming and early embryonic development in mice. Nat. Commun. 9, 1261. https://doi.org/10.1038/s41467-018-03008-2.
Zheng, H., Liu, C.C., Atagi, Y., Chen, X.F., Jia, L., Yang, L., et al., 2016. Opposing roles of the triggering receptor expressed on myeloid cells 2 and triggering receptor expressed on myeloid cells-like transcript 2 in microglia activation. Neurobiol. Aging 42, 132–141. https://doi.org/10.1016/j.neurobiolaging.2016.03.004.
Zhu, L., Skoultchi, A.I., 2001. Coordinating cell proliferation and differentiation. Curr. Opin. Genet. Dev. 11, 91–97. https://doi.org/10.1016/S0959-437X(00)00162-3.